JVI Accepts, published online ahead of print on 21 May 2014
J. Virol. doi:10.1128/JVI.00983-14

Effects of Toll-like Receptor Stimulation on Eosinophilic Infiltration in Lungs of BALB/c Mice Immunized with UV-inactivated Severe Acute Respiratory Syndrome-related Coronavirus Vaccine

Naoko Iwata-Yoshikawa[a], Akihiko Uda[b], Tadaki Suzuki[a], Yasuko Tsunetsugu-Yokota[c*], Yuko Sato[a], Shigeru Morikawa[b], Masato Tashiro[d], Tetsutaro Sata[a], Hideki Hasegawa[a], and Noriyo Nagata[a]#

Department of Pathology[a]; Department of Veterinary Science[b]; Department of Immunology[c]; and Influenza Virus Research Center[d], National Institute of Infectious Diseases, Tokyo, Japan

Running title: *TLR stimulation improves SARS-CoV vaccine efficacy*

#Address correspondence to Noriyo Nagata, nnagata@niid.go.jp

*Present address: Yasuko Tsunetsugu-Yokota, Tokyo University of Technology, Tokyo, Japan

10 Figures, 2 Tables, and 2 Supplementary Tables

Word count for the abstract, 231 words; importance, 130; text, 6437 words

Abstract

Severe acute respiratory syndrome-related coronavirus (SARS-CoV) is an emerging pathogen that causes severe respiratory illness. Whole UV-inactivated SARS-CoV (UV-V), bearing multiple epitopes and proteins, is a candidate vaccine against this virus. However, whole inactivated SARS vaccine that includes nucleocapsid protein is reported to induce eosinophilic infiltration in mouse lungs after challenge with live SARS-CoV. In this study, an ability of Toll-like receptor (TLR) agonists to reduce the side effects of UV-V vaccination in a 6-month-old adult BALB/c mouse model was investigated, using the mouse-passaged Frankfurt 1 isolate of SARS-CoV. Immunization of adult mice with UV-V, with or without alum, resulted in partial protection from lethal doses of SARS-CoV challenge, but extensive eosinophil infiltration in the lungs was observed. By contrast, TLR agonists added to UV-V vaccine, including lipopolysaccharide, polyU, and poly (I:C) (UV-V+TLR), strikingly reduced excess eosinophilic infiltration in the lungs and induced lower levels of interleukin-4 and -13 and eotaxin in the lungs than UV-V-immunization alone. Additionally, microarray analysis showed that genes associated with chemotaxis, eosinophil migration, eosinophilia, and cell movement, and the polarization of Th2 cells were up-regulated in UV-V- but not in UV-V+TLR-immunized mice. In particular,

CD11b+ cells in the lungs of UV-V-immunized mice showed the up-regulation of genes associated with the induction of eosinophils after challenge. These findings suggest that vaccine-induced eosinophil immunopathology in the lungs upon SARS-CoV infection could be avoided by the TLR agonist adjuvants.

38

39 **Importance**

40 Inactivated whole severe acute respiratory syndrome-related coronavirus (SARS-CoV)
41 vaccines induce neutralizing antibodies in mouse models, however, they also cause increased
42 eosinophilic immunopathology in the lungs upon SARS-CoV challenge. In this study, the ability
43 of adjuvant Toll-like receptor (TLR) agonists to reduce the side effects of UV-inactivated
44 SARS-CoV vaccination in a BALB/c mouse model was tested, using the mouse-passaged
45 Frankfurt 1 isolate of SARS-CoV. We found that TLR stimulation reduced the high level of
46 eosinophilic infiltration that occurred in the lungs of mice immunized with UV-inactivated
47 SARS-CoV. Microarray analysis revealed that genes associated with chemotaxis, eosinophil
48 migration, eosinophilia, and cell movement, and the polarization of Th2 cells were up-regulated
49 in UV-inactivated SARS-CoV-immunized mice. This study may be helpful for elucidating the
50 pathogenesis underlying eosinophilic infiltration resulting from immunization with inactivated
51 vaccine.

52

53 **Introduction**

54 Severe acute respiratory syndrome-related coronavirus (SARS-CoV), a cause of severe
55 respiratory illness, emerged in southern China in late 2002 and quickly spread to several
56 countries throughout Asia, Europe and North America by early 2003 (1-4). Although SARS has
57 not re-emerged since 2003, vaccination is the most likely mode of preventing future SARS-CoV
58 outbreaks, especially in individuals at high risk, such as healthcare workers. To date, no vaccine
59 is licensed for SARS-CoV. A SARS-CoV vaccine based on whole inactivated virions is easily
60 prepared and is expected to induce a broader spectrum of antibodies compared to recombinant
61 virus based vaccines expressing particular sets of SARS-CoV proteins. Although inactivated
62 whole SARS-CoV vaccines induce neutralizing antibodies in mouse models (5-10), they also
63 cause increased eosinophilic immunopathology in the lungs upon SARS-CoV challenge (11-14).
64 These reactions are thought to be caused by the incorporation of SARS-CoV nucleocapsid
65 protein (N) in vaccine formulations, which induces N-specific immune responses and enhances
66 eosinophilic immune pathology (11, 12, 15).

67 Enhanced eosinophilic immune pathology was also observed in the 1960s, when
68 formalin-inactivated respiratory syncytial virus (FI-RSV) vaccine combined with alum adjuvant

69 was injected intramuscularly into children to immunize them against RSV. In these trials, 80% of
70 immunized children were hospitalized and died of enhanced respiratory disease upon subsequent
71 RSV infection. Histologic examination of their lungs showed bronchoconstriction and severe
72 pneumonia with peribronchiolar eosinophils (16, 17). These findings suggest that FI-RSV
73 vaccination induced non-neutralizing, non-protective antibodies, with natural infection of RSV
74 causing a hypersensitivity response to viral antigens, characterized by bronchoconstriction and
75 severe pneumonia. The pathology of the enhanced respiratory disease upon subsequent RSV
76 infection are thought to be due to skewing of the immune response toward Th2, with eosinophils
77 having a key role in the progression of enhanced respiratory disease. The generation of
78 non-protective antibodies by the FI-RSV vaccine may have been due to poor Toll-like receptor
79 (TLR) stimulation (18).

80 Thus, TLR stimulation with an inactivated whole virion vaccine is thought to be crucial to
81 induce protective antibodies and to reduce eosinophilic responses. In this study, we evaluated the
82 efficacy and safety of UV-inactivated whole SARS-CoV (UV-V) in a model using BALB/c mice
83 and mouse-passaged SARS-CoV. We investigated the ability of adjuvant TLR agonists to reduce
84 the side effects of UV-V vaccination, such as enhanced eosinophilic immune pathology.
85

Materials and methods

Viruses and cells

Vero E6 cells, purchased from the American Type Cell Collection (Manassas, VA), were cultured in Eagle's minimal essential medium (MEM) containing 5% fetal bovine serum (FBS), 50 IU/ml penicillin G, and 50 µg/ml streptomycin. Stocks of the mouse-passaged Frankfurt 1 isolate of SARS-CoV, F-musX-VeroE6 (F-musX), were propagated and titrated on Vero E6 cells and cryopreserved at -80°C as previously described (19). Viral infectivity titers are expressed as 50% of the tissue culture infectious dose ($TCID_{50}$) /ml on Vero E6 cells, as calculated according to the Behrens-Kärber method. Work with infectious SARS-CoV was performed under biosafety level 3 conditions.

Preparation of UV-V

UV-V was prepared as previously described (6). Briefly, the HKU39849 isolate of SARS-CoV was amplified in Vero E6 cells, exposed to UV light (4.75 J/cm^2), and purified by sucrose density gradient centrifugation. Inactivation of the virus infectivity of UV-V was confirmed upon inoculation to Vero E6 cells.

Animal experiments

BALB/c female mice, purchased from Japan SLC Inc. (Shizuoka, Japan), were housed in an environmentally controlled specific pathogen-free animal facility. Animals were infected with SARS-CoV in biosafety level 3 animal facilities, according to the Animal Care and Use Committee of the National Institute of Infectious Diseases, Tokyo, Japan.

For immunization, 14-week-old BALB/c mice were subcutaneously injected in the back with 10 μg UV-V alone (UV-V), 10 μg UV-V plus 2 mg alum (Pierce, Rockford, Ill) (UV-V+Alum), or 10 μg UV-V plus TLR agonists (UV-V+TLR), and reimmunized 6–7 weeks later. The TLR agonists consisted of 1 μg lipopolysaccharide (LPS; Sigma-Aldrich, St. Louis, MO), 2.5 μg poly (I:C) (Invitrogen, San Diego, CA), and 0.1 μg polyU (Invitrogen) per immunization. Control mice were injected with phosphate buffered saline (PBS) with or without Alum.

At 8–10 days after the 2nd immunization, mice were anesthetized by intraperitoneal injection of a mixture of 1.0 mg ketamine and 0.02 mg xylazine in 0.1 ml/10 g body weight. The animals were subsequently inoculated in the left nostril with $10^{6.5}$ $TCID_{50}$ of F-musX in 30 μl, 1000-fold higher than the 50% lethal dose for adult BALB/c mice (n = 5–7 per group) (19).

A second vaccination experiment was performed to evaluate the long-term efficacy of TLR, with the vaccinated mice rested for 4 weeks before F-musX challenge. Ten-week-old BALB/c mice were vaccinated with 10 μg UV-V or 10 μg UV-V+TLR and boosted 6 weeks later. Four weeks afterwards, the animals were inoculated in the left nostril with $10^{6.5}$ $TCID_{50}$ in 30 μl of F-musX.

To mimic immunization with an attenuated vaccine, 25-week-old mice were administered intranasally with $10^{6.3}$ $TCID_{50}$ of the HKU39849 isolate in 20 μl, since HKU39849 was shown to be avirulent in adult mice. Control mice were injected with MEM intranasally. Fourteen days later, these mice were challenged intranasally with $10^{6.5}$ $TCID_{50}$ in 30 μl of F-musX.

Body weights were measured daily for 10 days, and the mice were sacrificed 3 or 10 days after challenge to analyze virus replication, hematology, cytokine expression, and pathology (n = 3–4 per group).

Virus titration.

To titrate a virus infectivity in lung homogenates, 10% (w/v) tissue homogenates of each lung were prepared in MEM containing 2% FBS, 50 IU/ml penicillin G, 50 μg/ml streptomycin,

and 2.5 μg/ml amphotericin B. Lung wash fluid was also collected for analysis of infectious virus titers.

Cytokine and chemokine profiling.

Inflammatory profiling of 10% (w/v) lung homogenates was performed using the Milliplex® Map assay (Millipore, MA), as described by the manufacturer. These assays can determine the concentrations of 18 cytokines and chemokines, including eotaxin, granulocyte macrophage colony-stimulating factor (GM-CSF), interferon (IFN) γ, interleukin (IL)-1β, IL-2, IL-4, IL-5, IL-6, IL-7, IL-10, IL-12 (p70), IL-13, interferon gamma-induced protein 10 (IP-10), neutrophil-related chemokine KC (KC), monocyte chemoattractant protein-1 (MCP-1), macrophage inflammatory protein-1α (MIP-1α), regulated and normal T cell expressed and secreted (RANTES), and tumor necrosis factor-α (TNF-α). Type I IFNs in 10% (w/v) lung homogenates obtained 3 and 10 days after inoculation were analyzed using mouse IFN-α and -β ELISA kits (PBL Interferon Source, Piscataway, NJ), according to the protocol described by the manufacturer.

SARS-CoV neutralizing assay

Blood was obtained from the tail vein of each mouse and allowed to clot. Sera were collected by centrifugation, and inactivated by incubation at 56°C for 30 min. One hundred $TCID_{50}$ aliquots of F-musX of SARS-CoV were incubated for 1 hour in the presence or absence of mice sera serially 2-fold diluted, and then added to confluent Vero E6 cell cultures in 96-well microtiter plates as described (20). The presence of a viral cytopathic effect was determined on day 3, and the titers of neutralizing antibody were determined as the reciprocal of the highest dilution at which cytopathic effect was not observed. The lowest and highest serum dilutions tested were 1:2 and 1:512, respectively.

Quantitative real-time reverse-transcription (RT)-PCR.

To assay type I IFN mRNA expression and viral genome copies during early phases of SARS-CoV infection, the left lobe of a lung from mice injected with UV-V (n=6), UV-V+TLR (n = 6), or PBS (n =3) was obtained 1 day after challenge and placed in RNA later solution (Ambion). RNA was extracted from the lung samples using RNeasy® mini kits (Qiagen, Hilden, Germany), according to the manufacturer's instructions.

166 Real-time one-step quantitative RT-PCR assays were used to detect IFN-α4, IFN-β, and
167 SARS-CoV mRNA using QuantiTect Probe RT-PCR kits (Qiagen, Valencia, CA) and an ABI
168 PRISM 7900HT Fast Real Time PCR System (Applied Biosystems, Foster City, CA). TaqMan
169 probes and primers are listed in Table 2. Reactions were incubated at 50°C for 30 minutes,
170 followed by 95°C for 15 minutes and thermal cycling, which consisted of 40 cycles of
171 denaturation at 94°C for 15 seconds, and annealing and extension at 60°C for 60 seconds. The
172 expression of each gene was normalized relative to that of β-actin mRNA, with the expression of
173 IFN-α4 and IFN-β mRNAs calculated as the $\log_{10}$ fold-change relative to PBS-injected and
174 challenged mice.

175

176 **Histopathology and immunohistochemistry**

177 Animals were anesthetized and perfused with 2 ml of 10% phosphate-buffered formalin (n
178 =3–4). Animals were necropsied within 12 hours of death, whereas moribund animals were
179 euthanized by excess isoflurane. All animals were subsequently examined histopathologically,
180 with 10% phosphate-buffered formalin injected into the trachea until the lungs inflated. Fixed
181 lung tissues were routinely embedded in paraffin, sectioned, and stained with hematoxylin and

eosin. Eosinophils were identified with a C.E.M. kit using Astra Blue/Vital New Red staining (DBS, Pleasanton, CA). For Astra Blue/Vital New Red stained slides, five 240-μm^2 sections in the extrabronchioles were assessed, and the eosinophils, neutrophils, lymphocytes, and macrophages counted were averaged per lung of each mouse. Immunohistochemical detection of SARS-CoV antigens was performed on paraffin-embedded sections, as previously described (19).

Isolation of CD11b positive (CD11b+) lung cells

Whole lungs were collected from mice 1 day after challenge with F-musX, and their CD11b+ cells were isolated by a modification of previous protocols (21). Briefly, mice were euthanized under excess anesthesia and the lungs were perfused via the left ventricle with 20 ml of PBS containing 10 U/ml of heparin (Novo Nordisk Pharma Ltd., Novo Alle, Denmark) to remove RBCs. The lungs were removed aseptically, cut into 1 mm pieces, and incubated in HEPES buffer containing collagenase D (2 mg/ml; Roche Applied Science, Mannheim, Germany) and bovine pancreatic deoxyribonuclease I (40 U/ml; Sigma-Aldrich) for 30 to 45 min at 37°C. Single cell suspensions were prepared by gently pushing the tissue through a 70 μm nylon screen, followed by washing and centrifugation at 2000 rpm. To isolate CD11b+ cells, the

198 single cell suspensions were washed with PBS containing 0.5% FBS (PBS-FBS), counted, and
199 incubated at the appropriate ratio with MACS CD11b microbeads (Miltenyi Biotec, Auburn, CA)
200 for 15 min at 4°C. After washing again with 10 ml of PBS-FBS, the cells were diluted in 3 ml of
201 PBS-FBS. Finally, the CD11b+ cells were separated by passing the antibody-coated cell
202 suspension over an MS-positive selection column on a SuperMACS magnetic cell separator
203 (Milteni Biotec). CD11b+ cells were collected by removing the column from the magnetic field
204 and then flushing it with PBS-FBS. Purity was checked by flow cytometry. To confirm the
205 morphology of the obtained cells, around 1 x 10^5 cells in 100 µl of PBS-FBS were centrifuged at
206 1000 rpm for 10 min onto glass slides using a Shandon cytocentrifuge (Thermo Fisher Scientific
207 Inc., Waltham, MA). These cells were stained with Giemsa and analyzed by microscopy.
208
209 **Flow cytometry analysis**
210 The lung CD11b+ cells were washed with PBS-FBS. After blocking Fc receptors by
211 incubating 1 µg of anti-mouse CD16/CD32 MAb (BD Pharmingen, San Jose, CA) per 10^6 cells
212 for 20 min on ice, the cells were stained for 30 min on ice with allophycocyanin
213 (APC)-conjugated anti-mouse CD11b (BioLegend Inc., San Diego, CA). The cells were washed

twice in PBS-FBS and fixed with 2% paraformaldehyde. Flow cytometry was performed on a FACS Canto II (Becton Dickinson, San Diego, CA), with the data analyzed using FlowJo software 8.7.1 (Treestar, Ashland, OR).

Microarray analysis

Microarray analysis was performed using left lung lobe tissue samples and CD11b+ cells in the lung, as described (22). Briefly, total RNA was extracted using an RNeasy® mini kit (Qiagen, Hilden, Germany), according to the manufacturer's instructions. RNA concentrations were measured with a ND-1000 spectrophotometer (Nanodrop Technologies, Wilmington, DE). The quality of the RNA samples was assessed spectroscopically and the quality of the intact RNA was assessed using an Agilent 2100 Bioanalyzer (Agilent Technologies, Inc., Palo Alto, CA). RNA samples with the highest RNA integrity number, of more than 7, as determined by the Bioanalyzer were used for microarray analysis. Two hundred micrograms (lung tissue) or 25 μg (CD11b+ cells) of total RNAs was used for amplification and labeled using a Low RNA Input Linear Amplification Kit (Agilent).

Individual cRNA samples were fragmented by incubation with fragmentation buffer and blocking agent at 60°C for 30 min (Gene Expression Hybridization Kit; (Agilent). These RNA samples were hybridized at 65°C for 17 h at 10 rounds per min to SurePrint G3 Mouse GE 8x60K Microarray (Agilent). Controls consisted of RNA samples from mice injected with PBS, applied in duplicate to the slides; single samples were applied for all other RNA samples. The microarray slides were washed with wash solutions 1 and 2 (Agilent), and acetonitrile (Wako, Osaka, Japan). The slides were scanned with a DNA microarray scanner (Agilent), the images were analyzed using Feature Extraction software (Agilent), and the data files were automatically exported. Data mining was performed with GeneSpring GX 12.1 (Agilent). Briefly, the text file exported by Feature Extraction software was imported into GeneSpring. The raw data were normalized per chip to the 75th percentile expression level and per gene to the median expression intensity of all samples. The samples of lung tissue were classified into four groups based on the treatment regimen: six mice each were immunized with UV-V, UV-V+TLR, and HKU39849, and three mice each were injected with PBS, yielding a total of six microarrays because the PBS samples were run in duplicate. CD11b+ cell samples were classified into four groups based on the treatment regimen: six mice each were infected with F-musX and immunized with UV-V or

UV-V+TLR, and six mice each were mock infected and immunized with UV-V or UV-V+TLR. Since the differences in individual gene expression within each group were small, all data are presented as the mean per group. Significant differences in gene expression between the UV-V and UV-V+TLR groups was assessed using one-way ANOVA, followed by Tukey's honestly significant difference post-hoc test and Benjamini-Hochberg correction test, with p values ≤ 0.05 considered statistically significant, and further filtered by $\geq$2-fold expression. Genes that met these criteria were characterized using Ingenuity Pathway Analysis (IPA) (Ingenuity Systems, Redwood City, CA) function annotations. All microarray slide hybridizations were performed using mouse oligonucleotide arrays (G4852A; Agilent). The microarray results have been deposited in Gene Expression Omnibus (GEO; http://www.ncbi.nlm.nih.gov/projects/geo/) and assigned accession numbers GSE44274 (lung tissue) and GSE50855 (CD11b + cells isolated from lung).

Statistical analysis.

Inter-group comparisons were performed by one-way ANOVA followed by Turkey's post-hoc test using GraphPad Prism 5 (GraphPad Software Inc., CA). *P* values less than 0.05 were considered statistically significant.

Results

Immunization with UV-V induces eosinophilic infiltrations in the lungs of adult mice after SARS-CoV challenge.

To confirm an induction of eosinophilic immunopathology by immunization with UV-V in the adult mouse model (19), 11 mice per group were immunized with the vaccine and challenged 10 days after boosting with the live virus. All of the control mice, injected with PBS and Alum (PBS+Alum), died of acute respiratory illness within 5 days after infection with the live virus (Fig. 1A). By contrast, UV-V+Alum-immunized mice showed mild illness, such as hunching, ruffled fur, and body weight loss, within 3 days of infection, and then recovered by day 5 (Fig. 1A). UV-V-immunized mice showed various levels of body weight loss and respiratory illness upon the virus challenge. One mouse immunized with UV-V and one immunized with UV-V+Alum died on day 5. Virus titers in the lungs on day 3 did not differ significantly among

UV-V-immunized, UV-V+Alum-immunized, and PBS+Alum-injected mice (n = 3 each) (Fig. 1B). By contrast, virus titers in lung wash fluid on day 3 were significantly lower in UV-V+Alum-immunized than in PBS+Alum-injected mice. On the day before challenge with live virus, the serum titers of neutralizing antibodies were significantly higher in UV-V+Alum- than in UV-V-immunized mice (n = 11 each) (Fig. 1C), but did not differ significantly after challenge. The PBS+Alum-injected mice did not show seroconversion against SARS-CoV after challenge. Microscopic analysis of the lung sections of mice at 3 days after infection showed a high level of eosinophil infiltration around the bronchi in UV-V- and UV-V+Alum-immunized mice (Fig.1D), whereas lymphocytes, macrophages and a few neutrophils had infiltrated into the lungs of PBS+Alum-injected mice (Fig. 1D). Eosinophil infiltration was severe on day 10 than on day 3 in UV-V- and UV-V+Alum-immunized mice. Histopathologically, both UV-V- and UV-V+Alum-immunized mice showed infiltration of inflammatory cells, including eosinophils, surrounding the bronchi and blood vessels on day 3 (n= 3 each) (Fig. 1E), consistent with previous results (13). We also investigated the lung pathology of the mice that died by day 5. Surprisingly, the lungs of both the UV-V- and UV-V+Alum-immunized mice showed high eosinophilic infiltration into areas surrounding the bronchi and blood vessels and severe

291 inflammatory infiltrations in the alveoli (Fig. 2). Immunohistochemical analysis showed that a
292 few SARS-CoV antigen-positive cells were present in the bronchiolar epithelial cells and alveolar
293 cells of the dead UV-V-immunized mouse, but were not present in cells of the dead
294 UV-V+Alum-immunized mouse (Fig. 2). Although the virus neutralization titers in the sera on
295 the day prior to virus challenge were 1:4 and 1:128 in the UV-V- and UV-V+Alum-immunized
296 mice, respectively, they were unable to survive following SARS-CoV infection. By contrast,
297 PBS+Alum-injected mice showed severe pulmonary edema, congestion, and hemorrhage, with
298 many viral antigen-positive cells in the alveoli 5 days after challenge. We considered that the
299 severe respiratory illness in the dead UV-V- and UV-V+Alum-immunized mice was caused by
300 an exacerbation of pulmonary inflammatory reactions due to UV-V acting as an inactivated RSV
301 vaccine (18). The excess pulmonary eosinophilic infiltration possibly resulted from host immune
302 responses rather than from a direct cytopathic effect caused by SARS-CoV replication.
303 Considering the excess eosinophilic immunopathology following SARS-CoV infection in
304 mice immunized with inactivated virus, we examined whether the natural course of immune
305 response elicited after non-lethal SARS-CoV infection resulted in excess eosinophil infiltration in
306 the lung of the re-infected mice. Mice were infected with the HKU39849 isolate, which induces

non-lethal infection of both young and adult BALB/c mice, and challenged with F-musX. None of the HKU39849-inoculated mice showed clinical illness, as assessed by the absence of ruffled fur, dyspnea, and weight loss, and all survived after F-musX challenge (Fig. 3A). Virus titers in the lungs of control mice were high on day 3 (10^8 $TCID_{50}$/g), although titers in the lungs and lung wash fluids of HKU39849-inoculated mice on days 3 and 10 after challenge were below the limit of detection (Fig. 3B). Virus neutralization titers in the sera on the day prior to virus challenge were higher than 1:16 (Fig. 3C). Histopathologically, the lungs of HKU39849-inoculated mice showed mild perivascular and peribronchiolar mononuclear cell infiltration on days 3 and 10 after the challenge (Fig. 3D, E). Most of these infiltrating cells were lymphocytes, with no eosinophils, and there were no cells positive for viral antigens in the lungs. By contrast, MEM-treated control mice showed severe respiratory illness and weight loss after F-musX infection, and succumbed to infection within 5 days (Fig. 3A). The lung pathology of these control mice was similar to that of PBS+Alum-injected mice following challenge with SARS-CoV (data not shown). Thus inoculation with HKU39849, mimicking immunization with attenuated live vaccine, provided a high level of protective immunity against SARS-CoV infection and elicited mild lymphocytic, but not eosinophil infiltration, in the lung after reinfection with F-musX.

Immunization with UV-V plus TLR agonists inhibits skewing to a Th2 response and high eosinophilic infiltration into the lungs of adult mice after challenge infection.

We hypothesized that the excess pulmonary eosinophilic infiltration observed in mice immunized with UV-V was due to poor Toll-like receptor (TLR) stimulation as shown in FI-RSV vaccination (18). TLR agonists were used to induce host immune responses, especially innate immune responses, to virus infection (23, 24). Recognition by TLRs induces innate immune responses and eventually leads to activation of antigen-specific immunity (23). In addition, inactivated RSV vaccine-induced pulmonary disease was resolved by the addition of TLR agonists in an RSV mouse model (18). Therefore, we investigated the effect of TLR agonists as an adjuvant during immunization with UV-V. Within 3 days of challenge infection, UV-V+TLR-immunized mice developed a clinical illness, characterized by weight loss, hunching, and ruffled fur, but recovered by day 4 (Fig. 4A). By day 10, the body weight of all mice had recovered to that before immunization, and no mice had died (Fig. 4B). The survival rates, weight loss and clinical illness of UV-V- and UV-V+TLR-immunized mice did not differ significantly. Viral titers in lung wash fluid, but not in the lungs, were significantly lower in

339 UV-V+TLR-immunized mice than in PBS-injected mice on day 3 p.i. (Fig. 4C). Both UV-V- and
340 UV-V+TLR-immunized mice showed seroconversion against SARS-CoV after the booster
341 injection, with the titers of neutralizing antibodies on day 10 tending to be higher in UV-V+TLR-
342 than in UV-V-immunized mice (Fig. 4D). Interestingly, slight eosinophilic infiltration was
343 observed in the lungs of UV-V+TLR-immunized mice on day 3, but not on day 10 (Fig. 4E). On
344 day 10, lymphocytes were the primary infiltrating cells around vessels in the lungs of these mice.
345 The numbers of eosinophils in the lungs were significantly lower in UV-V+TLR- than in
346 UV-V-immunized mice (Fig. 4F). Cytokine and chemokine responses were assessed in lung
347 homogenates of UV-V- and UV-V+TLR-immunized mice on days 3 and 10. The levels of the
348 Th2-related inflammatory cytokines IL-4 and IL-13 and the eosinophil-related chemokine eotaxin
349 (CCL11) were lower in UV-V+TLR- than in UV-V-immunized mice on days 3 and 10 (Fig. 5).
350 By contrast, the levels of IP-10 (CXCL10) and KC (CXCL1) tended to be higher in UV-V+TLR-
351 than in UV-V-immunized mice on day 3. There were no significant differences among UV-V-,
352 UV-V+TLR-immunized, and PBS+Alum-injected mice in the levels of other proinflammatory
353 cytokines and chemokines, including GM-CSF, IFN-γ, IL-12p70, IL-1b, IL-2, IL-5, IL-6, IL-7,
354 MCP-1, MIP-1α, RANTES, and TNF-α. These results indicate that TLR agonists are potent

355 adjuvants that inhibit the skewing of immune responses towards Th2 responses and block the
356 enhanced eosinophilic infiltration into the lungs that occurs after SARS-CoV infection.
357
358 **Immunization with UV-V plus TLR agonists induces IFN-β gene expression in the lungs**
359 **after challenge**
360 Stimulation of TLRs-3, -4, and -7 by TLR agonists induces type I IFNs, with the induction of
361 these type I IFNs being the most immediate antiviral host response to many viral infections (25).
362 To confirm the effect due to poly(I:C) injection before challenge in UV-V+TLR-immunized mice,
363 we employed quantitative real-time RT-PCR to assess mRNA expression levels in UV-V- and
364 UV-V+TLR-immunized mice (n = 6) 1 day after challenge. The amount of IFN-α4 mRNA did
365 not differ significantly in the lung tissues of UV-V- and UV-V+TLR-immunized mice. Although
366 IFN-β gene expression in the lungs was significantly higher in UV-V+TLR- than in
367 UV-V-immunized mice on day 1 (Fig. 6A), the viral copy number in the lungs of these mice did
368 not differ significantly (Fig. 6B). In addition, ELISA assays showed that IFNα and β in the sera
369 and lungs of UV-V- and UV-V+TLR- and PBS-infected mice were below the limits of detection 3
370 and 10 days after challenge.

371

372 **Presence of eosinophil infiltration in the lungs after both short and long interval**
373 **UV-V-immunization in response to virus challenge.**

374 A second vaccine experiment was performed to evaluate the long-term antiviral efficacy of
375 UV-V+TLR. Fourteen mice per group were immunized with UV-V and UV-V+TLR and boosted
376 6 weeks later. Four weeks after boosting, the mice were intranasally challenged with F-musX.
377 Both UV-V- and UV-V+TLR-immunized mice showed slight illness and mild loss of body
378 weight, but recovered by day 6 (Fig. 7A). Virus titers in the lungs and lung wash fluid on day 3
379 were below the limit of detection in both UV-V- and UV-V+TLR-immunized mice (Fig. 7B).
380 One day before challenge, the serum titers of neutralizing antibodies were higher in both sets of
381 immunized mice when compared with the previous experiment in Figure 4 (Fig. 7C).
382 Microscopic analysis of the lung sections of UV-V-immunized mice 3 days after challenge
383 showed eosinophil infiltration surrounding the bronchi and blood vessels (Fig. 7E), but the
384 number was lower in these mice than in the mice challenged in Figure 4 (Fig. 7D). Eosinophil
385 infiltration in the lung was lower on day 10 than on day 3 in UV-immunized mice. After long
386 intervals, the UV-V and UV-V+TLR immunized mice seroconverted to produce sufficient

neutralizing antibody against SARS-CoV infection. However, both short and long interval UV-V-immunization caused eosinophil infiltration in the lungs after challenge.

UV-V-immunized mice showed high expression of genes related to Th2 responses in the lungs after challenge.

To better understand the biological pathways by which UV-V-induced pulmonary eosinophilia occurs, we examined global transcriptional changes in mouse lungs. Gene expression profiling was performed using total RNAs from the lungs of mice immunized with UV-V, UV-V+TLR, PBS (as a mock vaccination), or HKU39849 (mimicking live attenuated vaccine) 1 day after F-musX inoculation. A total of 242 genes were differentially regulated between UV-V- and UV-V+TLR-immunized mice. These data are plotted as a heat map, in which each entry represents a gene expression value (Fig. 8A). The data for PBS-injected and HKU39849-inoculated mice were also plotted on a heat map. UV-V- and UV-V+TLR-immunized mice elicited different patterns of gene expression associated with immune responses after SARS-CoV infection. Two trends were observed on the heat maps. 242 genes showed changes in expression level, with 107 genes up-regulated and 135 genes

403 down-regulated in UV-V-immunized mice. Gene ontology analysis revealed that genes involved
404 in the function, proliferation, differentiation, activation and maturation of immune cells were
405 expressed similarly, whereas genes associated with chemotaxis, eosinophil migration,
406 eosinophilia, cell movement, and the polarization of Th2 cells were up-regulated in
407 UV-V-immunized mice (Table 1 and Supplementary Table 1) but down-regulated in
408 UV-V+TLR-immunized mice. Genes up-regulated in UV-V+TLR-immunized mice included
409 those associated with signaling of the proinflammatory cytokines TNF-α1 and 2, both of which
410 are regulated by TLRs, including TLR3 and TLR4 (Fig. 9). To assess the interconnection
411 between genes during the host response to virus infection after UV-V immunization, a functional
412 analysis approach was used to construct a graphic network of biologically related genes derived
413 from IPA. This network was constructed by including the 242 genes differentially regulated
414 between UV-V- and UV-V+TLR-immunized mice. Interestingly, this analysis yielded only one
415 network, consisting of 39 of the 242 genes. The gene encoding IL-4 is at the center of this
416 network (Fig. 8B). Network analysis revealed that differential gene regulation occurred
417 independently, including the up-regulation of the Th2-related chemokine thymus and
418 activation-regulated chemokine (also called CCL17), eotaxin-2 (CCL24), and IL-4 in

419 UV-V-immunized mice. The expression of the IL-4 and CCL24 genes was especially higher in
420 the lungs of UV-V- than of UV-V+TLR-immunized mice. These genes are associated with a
421 network involving attraction, chemotaxis, accumulation, and stimulation of eosinophils. In
422 addition, CCL17 and IL-4 are also associated with Th2 cell movement, homing, polarization and
423 arrest of proliferation. Most genes associated with "inflammation of the lungs" were unchanged
424 or down-regulated in UV-V- compared with UV-V+TLR-immunized mice, including Actin, beta
425 (ACTB), cathelicidin antimicrobial peptide (CAMP), coagulation factor X enzyme (F10),
426 inhibitor of kappa light polypeptide gene enhancer in B-cells, kinase epsilon (IKBKE),
427 interleukin 15 receptor alpha (IL-15RA) , IL-4, plasminogen activator, tissue (PLAT), spleen
428 focus forming virus proviral integration oncogene (SPI1), and TRAF family member-associated
429 NFκB activator (TANK) (Fig. 8B). Thus, both mRNA and protein assays for host immune
430 responses revealed that the expression of genes related to Th2 responses, especially IL-4, had a
431 key role in the excess eosinophilic immunopathology observed in the lungs of UV-V-immunized
432 mice after subsequent SARS-CoV infection. Such unwanted side effects could be avoided by
433 adding TLR antagonists as an adjuvant.
434

435 **CD11b+ cells in the lungs of UV-V-immunized mice show up-regulation of genes associated**
436 **with induction of eosinophils after challenge.**

437 In addition, gene expression analysis was analyzed in CD11b+ cells, including macrophages,
438 lymphocytes and granulocytes, which express TLRs (26, 27). The purity of CD11b+
439 cell-populations was confirmed by flow cytometry after magnetic bead separation and was
440 typically greater than 94% (Figure 10A and D). Microscopic examination revealed that most of
441 the sorted CD11b+ cells were mononuclear small and large cells, but also included polynuclear
442 cells (Figure 10B and E). A comparison of the gene expression profiles of CD11b+ cells from
443 UV-V- and UV-V+TLR-immunized mice showed that a total of 434 genes were differentially
444 regulated. To dissect the temporal behavior of key players involved in TLR signaling in more
445 detail, our data were analyzed using the IPA. Upstream Regulator Analysis showed that certain
446 genes were upstream regulators, including TLR3, TLR4, and polyI:C (Supplementary Table 2).
447 To better understand the relationships of these genes, pathway networks were built. Although
448 many networks could be constructed, we limited our investigation to the networks associated
449 with the TLR 3, 4, and 7 signaling pathways in order to understand the effect of treatment with
450 TLR agonists on CD11b+ cells. The network of differentially expressed genes related to TLR3,

TLR4, and polyI:C is shown in Figure 10 C and F; a network for TLR7 could not be built from these data. The network involving TLR3, TLR4, and polyI:C consisted of 37 genes, many of which were associated with cellular movement, hematological system development and function, immune cell trafficking, inflammatory response, and infectious disease. There was no difference in gene expression in UV-V-immunized and UV-V+TLR-immunized mice following mock infection. The levels of expression of genes encoding solute carrier family 5, member 5 (SLC5A5), interferon regulatory factor 1 (IRF1), interferon gamma-induced GTPase (Igtp), immunity-related GTPase family M member 2 (Irgm2), interferon inducible GTPase 1 (Iigp1), chemokine (C-X-C motif) ligand 9 (CXCL9), CD40, guanylate binding protein 4 (GBP4), and guanylate binding protein 2 (GBP2) were especially higher in CD11b+ cells from UV-V+TLR- than from UV-V-immunized mice. These genes were associated with cellular movement, recruitment of leukocytes, and maturation of antigen presenting cells. In contrast, CD11b+ cells from UV-V-immunized mice showed much more robust regulation of genes in this network than cells from UV-V+TLR-immunized mice. However, several of these genes, including those encoding CXCL2, plasminogen activator receptor (PLAUR), lactotransferrin (LTF), TNF-inducible gene 6 protein (TNFAIP6), CXCL9, and polyI:C RNA, have also been implicated

in eosinophil migration and eosinophilia of the airways. IPA analysis revealed that these genes were also up-regulated in CD11b+ cells from the lungs of UV-V-immunized mice.

Discussion

This study describes vaccine immunization, both with attenuated live and inactivated vaccines, and virus challenge using adult BALB/c mice and mouse-passaged SARS-CoV. This model is useful in the evaluation of efficacies and side effects of vaccine candidates. Several strategies have been considered for vaccination against SARS-CoV (reviewed in 28). Spike protein, but not envelope, membrane, or N proteins, protects vaccinated animals from SARS-CoV infection by inducing neutralizing antibodies (29-31) and strong cellular immunity. Antibodies detected in the sera of patients infected with SARS-CoV were directed against at least eight different proteins and bound to viral membranes (32). These findings indicate that multiple epitopes and proteins may be targets of protective antibodies. Although vaccination with attenuated viruses are more efficacious than those with inactivated viruses due to their persistence in the host, attenuated viruses carry the risk of reversion of virulence or recombination repair (33). Due to safety concerns, it is often difficult to gain regulatory approval of attenuated vaccines

without strong proof that the threat of disease is sufficient to warrant their use. This threshold has not yet been met for SARS, although some interesting attenuated mutants have been developed (34-36). By contrast, inactivated vaccines do not carry risks of mutating and reverting back to their virulent forms. UV-V virions have been successful due to large-scale production, the presentation of multiple epitopes, and the generation of high levels of humoral immunity in young BALB/c mice injected subcutaneously (37). However, SARS-CoV challenge has not been tested in more vulnerable animals.

In this study, we successfully evaluated the efficacy of UV-inactivated whole virion immunization in a lethal adult mouse model of SARS-CoV infection. Adult BALB/c mice immunized with UV-V failed to inhibit viral infection and replication within the lungs on day 3. This was one cause of death after subsequent SARS-CoV infection and of enhanced lung immunopathology characterized by increased infiltration by eosinophils. These findings are consistent with studies of vaccine formulations incorporating SARS-CoV N protein and also SARS-CoV doubly inactivated with formalin and UV irradiation (11-14). An excessive host immune response against the N protein of SARS-CoV enhances eosinophilic infiltration into the lungs, resulting in a failure to inhibit viral replication, and skewing the immune response toward

499 Th2 responses (11-14). Similar lung pathology has also been observed in humans vaccinated with
500 FI-RSV followed by RSV infection (38, 39), with the Th2-skewed cytokine profile also a
501 hallmark of RSV vaccine-enhanced disease (40). The Th2-skewed cytokine profile is shown to be
502 reduced only when the functions of IL-4 and IL-13, both Th2 cytokines, are blocked in
503 FI-RSV-immunized mice (41, 42), indicating that both IL-4 and IL-13 promote the development
504 of pulmonary eosinophilia upon RSV challenge of FI-RSV-immunized mice. High levels of Th2
505 cytokines, including IL-4 and IL-13, and the up-regulation of genes associated with Th2 cell
506 migration were observed in the lungs of UV-V-immunized mice, suggesting that the
507 UV-V-specific immune response occurs in a manner similar to that of the FI-RSV vaccine.
508 Furthermore, a few UV-V-immunized mice were unable to produce protective neutralizing
509 antibodies and died on day 5 after challenge, showing severe inflammation including high
510 eosinophilia in the lungs. Interestingly, a UV-V+Alum-immunized mouse produced high titers of
511 neutralizing antibodies in serum but died of eosinophilic pneumonia in this study. Vaccination
512 with UV-inactivated virions of other viruses may carry a potential for dangerous clinical
513 complications, similar to those observed for inactivated RSV vaccine. Pulmonary eosinophilia is
514 a hallmark of an aberrant hypersensitivity response to FI-RSV (43). A recent study using

515 eosinophil-deficient mice found that eosinophils did not contribute to RSV vaccine-enhanced
516 pulmonary disease (44). By contrast, another study using mouse pneumonia virus, resulting in
517 severe RSV, found that eosinophils did not promote virus clearance (45). The mechanism of
518 vaccine-induced eosinophilia has not been determined, with no consensus as to whether
519 eosinophils potentially contribute to protection or enhance lung immunopathology subsequent to
520 respiratory infection.

521 Vaccine failure in RSV enhanced respiratory disease was thought to be due to formalin
522 disruption of protective antigens. However, this lack of protection was not due to
523 formalin-induced alterations but to low antibody avidity for protective epitopes resulting from
524 poor TLR stimulation (18). To mimic live attenuated vaccine, mice were inoculated with
525 HKU39849, that completely protected them from subsequent SARS-CoV infection. Moreover,
526 these mice did not display enhanced eosinophilic infiltration in the lungs. In addition, all
527 mock-vaccinated mice died but did not show evidence of eosinophilia. TLRs are critical to
528 sensing invading microorganisms. Pathogen recognition by TLRs provokes the rapid activation
529 of innate immunity, leading to effective adaptive immunity (23). Despite the protective effects of
530 TLRs upon infection, faulty TLR signaling is increasingly implicated in the pathogenesis of

allergic diseases (46, 47). We hypothesized that vaccination with UV-V was unable to generate effective immunity against SARS-CoV infection because of poor TLR stimulation, which may be enough when SARS-CoV natural infection occurs. In fact, immunizing mice with UV-V, together with the TLR agonists, poly(I:C) (a TLR3 agonist), LPS (a TLR4 agonist) and polyU (a TLR7 agonist), as an adjuvant, produced effective antibodies and inhibited excess eosinophilic immunopathology. The innate immunomodulatory activity in response to live and inactivated SARS-CoV is not well understood. However, mouse models of related CoV infection have suggested protective roles for TLR4 (48) and myeloid differentiation factor 88 (MyD88) (49), whereas TLR3 and TLR7 may be important for viral clearance through the production of type I IFN (50, 51).

Intranasal injection of the TLR agonist poly (I:C) into aged mice provided a high level of protection against SARS-CoV infection (51). Indeed, higher IFN-β gene expression on day 1 p.i. was seen in the lungs of UV-V+TLR- than in those of UV-V-immunized mice. UV-V+TLR, but not UV-V, immunization primed the cells that expressed IFN-β after SARS-CoV infection. IFN-β was induced directly after sendai virus infection in a murine model, leading to the expression of IFN-α genes (52). Although viral copy numbers in the lungs were similar in both groups 1 day

after challenge, viral titers differed significantly in the lung wash fluid of UV-V+TLR- and PBS-injected mice on day 3. Virus excretion into the lungs of UV-V+TLR-immunized mice on day 3 may be inhibited by IFN-β gene expression. The type I IFNs not only play an important role in the innate immune response but also enhance Th1-type responses (53). Higher IFN-β gene expression in UV-V+TLR-immunized mice may therefore contribute to the production of Th1 cytokines after viral infection. To assess the efficacy of vaccination the mice, we demonstrated both short and long interval UV-V-immunization on virus challenge. The titer of neutralizing antibodies was higher after a longer period of time, and these antibodies were sufficiently protective against SARS-CoV infection. However, eosinophil infiltration in the lungs occurred in the UV-V-immunized mice.

Mice immunized with inactivated RSV plus TLR agonists produced mature antibodies following TLR stimulation, preventing enhanced respiratory disease (18). These findings suggest that TLR stimulation during immunization with UV-V plays a key role in reducing eosinophil infiltration into the lungs, with strong TLR stimulation by TLR agonists shifting the host immune response in the lungs from Th2 to Th1. In line with this, our microarray analysis showed that several genes downstream of TLR3 and TLR4 signaling were markedly up-regulated in

563 UV-V+TLR- compared with UV-V-immunized mice on day 1 after subsequent SARS-CoV
564 infection. Furthermore, IPA analysis of CD11b+ cells isolated from the lungs of
565 UV-V+TLR-immunized mice showed up-regulation of genes associated with cellular movement
566 and maturation of antigen-presenting cells in the TLR3 and TLR4 signaling pathways. This
567 finding indicated that UV-V+TLR, but not UV-V, immunization may prime effective innate
568 immune responses against SARS-CoV infection in mice due to the intensity of TLR stimulation.

569 To our knowledge, this is the first study to show that vaccination with UV-inactivated whole
570 virions plus TLR agonists provides protection against SARS-CoV infection without strong Th2
571 skewing; TLR stimulation reduced the high level of eosinophilic infiltration that occurred in the
572 lungs of mice immunized with UV-V. TLR agonists are approved for human use (54), and
573 several are currently in preclinical development for use as vaccine adjuvants (55). Further studies
574 regarding the association of TLR stimulation with protective immunity to SARS-CoV infection,
575 the indication that eosinophils contribute to the negative sequelae of disease, and the mechanisms
576 of eosinophil recruitment to lung tissue are required.

577

578 **Acknowledgements**

579 This work was supported by a Grant-in Aid for Young Scientist (B) no. 22790444 from the Japan
580 Society for the Promotion of Science, and Grant-in Aid for research on emerging and
581 re-emerging infectious diseases, H23-Shinko-Ippan-007, and H25-Shinko-Wakate-004 from the
582 Ministry of Health, Labor, and Welfare, Japan. We thank our colleagues at the institute,
583 especially Ms. Ayako Harashima and Ms. Mihoko Fujino for their technical assistance, and Dr.
584 Shin-ichi Tamura for valuable discussions.

585

586 **References**

587 1. **Drosten C, Gunther S, Preiser W, van der Werf S, Brodt HR, Becker S, Rabenau H,**
588 **Panning M, Kolesnikova L, Fouchier RA, Berger A, Burguiere AM, Cinatl J,**
589 **Eickmann M, Escriou N, Grywna K, Kramme S, Manuguerra JC, Muller S,**
590 **Rickerts V, Sturmer M, Vieth S, Klenk HD, Osterhaus AD, Schmitz H, Doerr HW.**
591 2003. Identification of a novel coronavirus in patients with severe acute respiratory
592 syndrome. N. Engl. J. Med. **348:**1967-1976.
593 2. **Ksiazek TG, Erdman D, Goldsmith CS, Zaki SR, Peret T, Emery S, Tong S, Urbani**
594 **C, Comer JA, Lim W, Rollin PE, Dowell SF, Ling AE, Humphrey CD, Shieh WJ,**
595 **Guarner J, Paddock CD, Rota P, Fields B, DeRisi J, Yang JY, Cox N, Hughes JM,**
596 **LeDuc JW, Bellini WJ, Anderson LJ.** 2003. A novel coronavirus associated with severe
597 acute respiratory syndrome. N. Engl. J. Med. **348:**1953-1966.
598 3. **Peiris JSM, Lai ST, Poon LLM, Guan Y, Yam LYC, Lim W, Nicholls J, Yee WKS,**
599 **Yan WW, Cheung MT, Cheng VCC, Chan KH, Tsang DNC, Yung RWH, Ng TK,**
600 **Yuen KY.** 2003. Coronavirus as a possible cause of severe acute respiratory syndrome.
601 The Lancet **361:**1319-1325.
602 4. **Rota PA, Oberste MS, Monroe SS, Nix WA, Campagnoli R, Icenogle JP, Penaranda**
603 **S, Bankamp B, Maher K, Chen MH, Tong S, Tamin A, Lowe L, Frace M, DeRisi JL,**
604 **Chen Q, Wang D, Erdman DD, Peret TC, Burns C, Ksiazek TG, Rollin PE, Sanchez**
605 **A, Liffick S, Holloway B, Limor J, McCaustland K, Olsen-Rasmussen M, Fouchier**
606 **R, Gunther S, Osterhaus AD, Drosten C, Pallansch MA, Anderson LJ, Bellini WJ.**
607 2003. Characterization of a novel coronavirus associated with severe acute respiratory
608 syndrome. Science **300:**1394-1399.
609 5. **He Y, Zhou Y, Siddiqui P, Jiang S.** 2004. Inactivated SARS-CoV vaccine elicits high
610 titers of spike protein-specific antibodies that block receptor binding and virus entry.
611 Biochem. Biophys. Res. Commun. **325:**445-452.
612 6. **Takasuka N, Fujii H, Takahashi Y, Kasai M, Morikawa S, Itamura S, Ishii K,**
613 **Sakaguchi M, Ohnishi K, Ohshima M, Hashimoto S, Odagiri T, Tashiro M,**
614 **Yoshikura H, Takemori T, Tsunetsugu-Yokota Y.** 2004. A subcutaneously injected
615 UV-inactivated SARS coronavirus vaccine elicits systemic humoral immunity in mice. Int.
616 Immunol. **16:**1423-1430.

7. **Tang L, Zhu Q, Qin E, Yu M, Ding Z, Shi H, Cheng X, Wang C, Chang G, Zhu Q, Fang F, Chang H, Li S, Zhang X, Chen X, Yu J, Wang J, Chen Z.** 2004. Inactivated SARS-CoV vaccine prepared from whole virus induces a high level of neutralizing antibodies in BALB/c mice. DNA Cell Biol. **23:**391-394.
8. **Xiong S, Wang YF, Zhang MY, Liu XJ, Zhang CH, Liu SS, Qian CW, Li JX, Lu JH, Wan ZY, Zheng HY, Yan XG, Meng MJ, Fan JL.** 2004. Immunogenicity of SARS inactivated vaccine in BALB/c mice. Immunol. Lett. **95:**139-143.
9. **Qu D, Zheng B, Yao X, Guan Y, Yuan ZH, Zhong NS, Lu LW, Xie JP, Wen YM.** 2005. Intranasal immunization with inactivated SARS-CoV (SARS-associated coronavirus) induced local and serum antibodies in mice. Vaccine **23:**924-931.
10. **Zhang CH, Lu JH, Wang YF, Zheng HY, Xiong S, Zhang MY, Liu XJ, Li JX, Wan ZY, Yan XG, Qi SY, Cui Z, Zhang B.** 2005. Immune responses in Balb/c mice induced by a candidate SARS-CoV inactivated vaccine prepared from F69 strain. Vaccine **23:**3196-3201.
11. **Deming D, Sheahan T, Heise M, Yount B, Davis N, Sims A, Suthar M, Harkema J, Whitmore A, Pickles R, West A, Donaldson E, Curtis K, Johnston R, Baric R.** 2006. Vaccine efficacy in senescent mice challenged with recombinant SARS-CoV bearing epidemic and zoonotic spike variants. PLoS Med **3:**2359-2375.
12. **Yasui F, Kai C, Kitabatake M, Inoue S, Yoneda M, Yokochi S, Kase R, Sekiguchi S, Morita K, Hishima T, Suzuki H, Karamatsu K, Yasutomi Y, Shida H, Kidokoro M, Mizuno K, Matsushima K, Kohara M.** 2008. Prior immunization with severe acute respiratory syndrome (SARS)-associated coronavirus (SARS-CoV) nucleocapsid protein causes severe pneumonia in mice infected with SARS-CoV. J. Immunol. **181:**6337-6348.
13. **Bolles M, Deming D, Long K, Agnihothram S, Whitmore A, Ferris M, Funkhouser W, Gralinski L, Totura A, Heise M, Baric RS.** 2011. A double-inactivated severe acute respiratory syndrome coronavirus vaccine provides incomplete protection in mice and induces increased eosinophilic proinflammatory pulmonary response upon challenge. J. Virol. **85:**12201-12215.
14. **Tseng CT, Sbrana E, Iwata-Yoshikawa N, Newman PC, Garron T, Atmar RL, Peters CJ, Couch RB.** 2012. Immunization with SARS coronavirus vaccines leads to pulmonary immunopathology on challenge with the SARS virus. PloS one **7:**e35421.
15. **Neuman BW, Adair BD, Yoshioka C, Quispe JD, Orca G, Kuhn P, Milligan RA,**

Yeager M, Buchmeier MJ. 2006. Supramolecular architecture of severe acute respiratory syndrome coronavirus revealed by electron cryomicroscopy. J. Virol. **80:**7918-7928.

16. **Kim HW, Canchola JG, Brandt CD, Pyles G, Chanock RM, Jensen K, Parrott RH.** 1969. Respiratory syncytial virus disease in infants despite prior administration of antigenic inactivated vaccine. Am. J. Epidemiol. **89:**422-434.

17. **Olson MR, Varga SM.** 2008. Pulmonary immunity and immunopathology: lessons from respiratory syncytial virus. Expert review of vaccines **7:**1239-1255.

18. **Delgado MF, Coviello S, Monsalvo AC, Melendi GA, Hernandez JZ, Batalle JP, Diaz L, Trento A, Chang HY, Mitzner W, Ravetch J, Melero JA, Irusta PM, Polack FP.** 2009. Lack of antibody affinity maturation due to poor Toll-like receptor stimulation leads to enhanced respiratory syncytial virus disease. Nat. Med. **15:**34-41.

19. **Nagata N, Iwata N, Hasegawa H, Fukushi S, Harashima A, Sato Y, Saijo M, Taguchi F, Morikawa S, Sata T.** 2008. Mouse-passaged severe acute respiratory syndrome-associated coronavirus leads to lethal pulmonary edema and diffuse alveolar damage in adult but not young mice. Am. J. Pathol. **172:**1625-1637.

20. **Nagata N, Iwata N, Hasegawa H, Sato Y, Morikawa S, Saijo M, Itamura S, Saito T, Ami Y, Odagiri T, Tashiro M, Sata T.** 2007. Pathology and virus dispersion in cynomolgus monkeys experimentally infected with severe acute respiratory syndrome coronavirus via different inoculation routes. Int. J. Exp. Pathol. **88:**403-414.

21. **Zhang X, Goncalves R, Mosser DM.** 2008. The isolation and characterization of murine macrophages. Current protocols in immunology / edited by John E. Coligan ... [et al.] **Chapter 14:**Unit 14 11.

22. **Sugiura N, Uda A, Inoue S, Kojima D, Hamamoto N, Kaku Y, Okutani A, Noguchi A, Park CH, Yamada A.** 2011. Gene expression analysis of host innate immune responses in the central nervous system following lethal CVS-11 infection in mice. Japanese journal of infectious diseases **64:**463-472.

23. **Kaisho T, Akira S.** 2002. Toll-like receptors as adjuvant receptors. Biochim. Biophys. Acta **1589:**1-13.

24. **Pashine A, Valiante NM, Ulmer JB.** 2005. Targeting the innate immune response with improved vaccine adjuvants. Nat. Med. **11:**S63-68.

25. **O'Neill LA, Bowie AG.** 2007. The family of five: TIR-domain-containing adaptors in Toll-like receptor signalling. Nature reviews. Immunology **7:**353-364.

26. **O'Mahony DS, Pham U, Iyer R, Hawn TR, Liles WC.** 2008. Differential constitutive and cytokine-modulated expression of human Toll-like receptors in primary neutrophils, monocytes, and macrophages. International journal of medical sciences **5:**1-8.

27. **Applequist SE, Wallin RP, Ljunggren HG.** 2002. Variable expression of Toll-like receptor in murine innate and adaptive immune cell lines. Int. Immunol. **14:**1065-1074.

28. **Roper RL, Rehm KE.** 2009. SARS vaccines: where are we? Expert review of vaccines **8:**887-898.

29. **Buchholz UJ, Bukreyev A, Yang L, Lamirande EW, Murphy BR, Subbarao K, Collins PL.** 2004. Contributions of the structural proteins of severe acute respiratory syndrome coronavirus to protective immunity. Proc. Natl. Acad. Sci. U. S. A. **101:**9804-9809.

30. **Bukreyev A, Lamirande EW, Buchholz UJ, Vogel LN, Elkins WR, St Claire M, Murphy BR, Subbarao K, Collins PL.** 2004. Mucosal immunisation of African green monkeys (Cercopithecus aethiops) with an attenuated parainfluenza virus expressing the SARS coronavirus spike protein for the prevention of SARS. Lancet **363:**2122-2127.

31. **Ishii K, Hasegawa H, Nagata N, Mizutani T, Morikawa S, Suzuki T, Taguchi F, Tashiro M, Takemori T, Miyamura T, Tsunetsugu-Yokota Y.** 2006. Induction of protective immunity against severe acute respiratory syndrome coronavirus (SARS-CoV) infection using highly attenuated recombinant vaccinia virus DIs. Virology **351:**368-380.

32. **Guo JP, Petric M, Campbell W, McGeer PL.** 2004. SARS corona virus peptides recognized by antibodies in the sera of convalescent cases. Virology **324:**251-256.

33. **Hanley KA.** 2011. The double-edged sword: How evolution can make or break a live-attenuated virus vaccine. Evolution **4:**635-643.

34. **DeDiego ML, Alvarez E, Almazan F, Rejas MT, Lamirande E, Roberts A, Shieh WJ, Zaki SR, Subbarao K, Enjuanes L.** 2007. A severe acute respiratory syndrome coronavirus that lacks the E gene is attenuated in vitro and in vivo. J. Virol. **81:**1701-1713.

35. **Dediego ML, Pewe L, Alvarez E, Rejas MT, Perlman S, Enjuanes L.** 2008. Pathogenicity of severe acute respiratory coronavirus deletion mutants in hACE-2 transgenic mice. Virology **376:**379-389.

36. **Lamirande EW, DeDiego ML, Roberts A, Jackson JP, Alvarez E, Sheahan T, Shieh WJ, Zaki SR, Baric R, Enjuanes L, Subbarao K.** 2008. A live attenuated severe acute

713 respiratory syndrome coronavirus is immunogenic and efficacious in golden Syrian
714 hamsters. J. Virol. **82:**7721-7724.
715 37. **Tsunetsugu-Yokota Y.** 2008. Large-scale preparation of UV-inactivated SARS
716 coronavirus virions for vaccine antigen. Methods Mol. Biol. **454:**119-126.
717 38. **Hancock GE, Speelman DJ, Heers K, Bortell E, Smith J, Cosco C.** 1996. Generation
718 of atypical pulmonary inflammatory responses in BALB/c mice after immunization with
719 the native attachment (G) glycoprotein of respiratory syncytial virus. J. Virol.
720 **70:**7783-7791.
721 39. **De Swart RL, Kuiken T, Timmerman HH, van Amerongen G, Van Den Hoogen BG,**
722 **Vos HW, Neijens HJ, Andeweg AC, Osterhaus AD.** 2002. Immunization of macaques
723 with formalin-inactivated respiratory syncytial virus (RSV) induces
724 interleukin-13-associated hypersensitivity to subsequent RSV infection. J. Virol.
725 **76:**11561-11569.
726 40. **Johnson TR, Varga SM, Braciale TJ, Graham BS.** 2004. Vbeta14(+) T cells mediate
727 the vaccine-enhanced disease induced by immunization with respiratory syncytial virus
728 (RSV) G glycoprotein but not with formalin-inactivated RSV. J. Virol. **78:**8753-8760.
729 41. **Johnson TR, Graham BS.** 1999. Secreted respiratory syncytial virus G glycoprotein
730 induces interleukin-5 (IL-5), IL-13, and eosinophilia by an IL-4-independent mechanism.
731 J. Virol. **73:**8485-8495.
732 42. **Johnson TR, Parker RA, Johnson JE, Graham BS.** 2003. IL-13 is sufficient for
733 respiratory syncytial virus G glycoprotein-induced eosinophilia after respiratory syncytial
734 virus challenge. J. Immunol. **170:**2037-2045.
735 43. **Rosenberg HF, Dyer KD, Domachowske JB.** 2009. Respiratory viruses and eosinophils:
736 exploring the connections. Antiviral Res. **83:**1-9.
737 44. **Castilow EM, Legge KL, Varga SM.** 2008. Cutting edge: Eosinophils do not contribute
738 to respiratory syncytial virus vaccine-enhanced disease. J. Immunol. **181:**6692-6696.
739 45. **Percopo CM, Qiu Z, Phipps S, Foster PS, Domachowske JB, Rosenberg HF.** 2009.
740 Pulmonary eosinophils and their role in immunopathologic responses to
741 formalin-inactivated pneumonia virus of mice. J. Immunol. **183:**604-612.
742 46. **Horner AA, Raz E.** 2003. Do microbes influence the pathogenesis of allergic diseases?
743 Building the case for Toll-like receptor ligands. Curr. Opin. Immunol. **15:**614-619.
744 47. **Vercelli D.** 2006. Mechanisms of the hygiene hypothesis--molecular and otherwise. Curr.

745 Opin. Immunol. **18:**733-737.
746 48. **Khanolkar A, Hartwig SM, Haag BA, Meyerholz DK, Harty JT, Varga SM.** 2009.
747 Toll-like receptor 4 deficiency increases disease and mortality after mouse hepatitis virus
748 type 1 infection of susceptible C3H mice. J. Virol. **83:**8946-8956.
749 49. **Sheahan T, Morrison TE, Funkhouser W, Uematsu S, Akira S, Baric RS, Heise MT.**
750 2008. MyD88 is required for protection from lethal infection with a mouse-adapted
751 SARS-CoV. PLoS Pathog **4:**1-12.
752 50. **Cervantes-Barragan L, Zust R, Weber F, Spiegel M, Lang KS, Akira S, Thiel V,**
753 **Ludewig B.** 2007. Control of coronavirus infection through plasmacytoid
754 dendritic-cell-derived type I interferon. Blood **109:**1131-1137.
755 51. **Zhao J, Wohlford-Lenane C, Zhao J, Fleming E, Lane TE, McCray PB, Jr., Perlman**
756 **S.** 2012. Intranasal treatment with poly(I*C) protects aged mice from lethal respiratory
757 virus infections. J. Virol. **86:**11416-11424.
758 52. **Erlandsson L, Blumenthal R, Eloranta ML, Engel H, Alm G, Weiss S, Leanderson T.**
759 1998. Interferon-beta is required for interferon-alpha production in mouse fibroblasts.
760 Curr. Biol. **8:**223-226.
761 53. **Biron CA.** 1998. Role of early cytokines, including alpha and beta interferons
762 (IFN-alpha/beta), in innate and adaptive immune responses to viral infections. Semin.
763 Immunol. **10:**383-390.
764 54. **Kanzler H, Barrat FJ, Hessel EM, Coffman RL.** 2007. Therapeutic targeting of innate
765 immunity with Toll-like receptor agonists and antagonists. Nat. Med. **13:**552-559.
766 55. **Horscroft NJ, Pryde DC, Bright H.** 2012. Antiviral applications of Toll-like receptor
767 agonists. J. Antimicrob. Chemother. **67:**789-801.
768 56. **Keyaerts E, Vijgen L, Maes P, Duson G, Neyts J, Van Ranst M.** 2006. Viral load
769 quantitation of SARS-coronavirus RNA using a one-step real-time RT-PCR. Int. J. Infect.
770 Dis. **10:**32-37.
771

772 Table 1 Top 5 of biological function categories by IPA in early response of mice immunized
773 with UV-V and UV-V+TLR subsequently challenged with SARS-CoV.
774

	Functions Annotation	*P*-value
UV-V	Eosinophil	7E-5 – 2E-2
	Function, proliferation, differentiation, activation and maturation of immune cells	6E-5 – 3E-2
	Th2	6E-5 – 1E-2
	Cell movement of immune cells	5E-5 – 3E-2
	Responses to pathogen	3E 5 – 3E-2
UV-V+TLR	Cell movement of immune cells	8E-6 – 3E-3
	Function, proliferation, differentiation, activation and maturation of immune cells	6E-5 – 3E-2
	Eosinophil	2E-2 – 1E-2
	Responses to pathogen	1E-4 – 2E-2
	Th2	-

775
776
777
778
779

780 Table 2 Primers and probes for quantitative real-time RT-PCR

Target	Sequences
IFN-α4	
Forward	CAACTCTACTAGACTCATTCTGCAAT
Reverse	AGAGGAGGTTCCTGCATCACA
Probe	ACCTCCATCAGCAGCTCAATGACCTCAAA
IFN-β	
Forward	GCTCCTGGAGCAGCTGAATG
Reverse	TCCGTCATCTCCATAGGGATCT
Probe	TCAACCTCACCTACAGGGCGGACTTC
SARS-CoV N gene	
(Reference 56)	
Forward	AGGAACTGGCCCAGAAGCTT
Reverse	AACCCATACGATGCCTTCTTTG
Probe	ACTTCCCTACGGCGCTA
β-actin	
Forward	ACGGCCAGGTCATCACTATTG
Reverse	CAAGAAGGAAGGCTGGAAAAGA
Probe	CAACGAGCGGTTCCGATGCCC

781

782

783

784 **Figure legends**

785

786 **Figure 1. Immunization with UV-V induces eosinophilic immune pathology in adult mice**
787 **after SARS-CoV challenge.** Adult female BALB/c mice were vaccinated with UV-V, UV-V
788 with Alum (UV-V+Alum), or vehicle (PBS with Alum, PBS+Alum) and subsequently challenged
789 with 1000 $TCID_{50}$ of F-musX. (A) Body weight changes following the challenge inoculation (n =
790 5). Dead mice are marked with crosses. Error bars indicate standard deviation. Significant
791 differences ($p < 0.05$, one-way ANOVA) between groups are marked with an asterisk. (B) Virus
792 titers in the lungs and lung wash fluids on day 3 post-challenge (n = 3). The dashed line indicates
793 the limit of detection ($10^{1.5}$ $TCID_{50}$/ml). Error bars indicate standard deviation. Significant
794 differences ($p < 0.05$, one-way ANOVA) between groups are marked with an asterisk. (C)
795 Neutralizing serum antibody titers against SARS-CoV on days 50, 29, and 1 before challenge (n
796 = 11), and on days 3 and 10 after challenge (n = 5–6). Serum samples were 2-fold serially diluted
797 beginning at 1:2. Error bars indicate standard deviation. Significant differences ($p < 0.05$,
798 one-way ANOVA) between groups are marked with an asterisk. (D) Numbers of lymphocytes,

799 macrophages, neutrophils and eosinophils in lung sections (n = 3) on day 3 after challenge. Five
800 240-μm^2 regions in the extrabronchioles of lung per mouse were examined at 40× magnification.
801 Asterisks indicate p <0.05 by the Bonferroni test. Error bars indicate standard deviation. (E)
802 Representative images of lung sections from UV-V- and UV+Alum-immunized mice on day 10
803 post-challenge. Hematoxylin and eosin (magnification, 10×) and C.E.M. kit staining (inset,
804 magnification, 100×). Br, bronchi; *, blood vessel.
805
806 **Figure 2. Histopathological findings in the lungs of dead mice after SARS-CoV challenge.**
807 Lungs were obtained for pathologic examination (A, C, and E) and immunohistochemical
808 analysis of SARS-CoV virus antigens (B, D, F) from mice that died 5 days after challenge. Br,
809 bronchi; *, blood vessel. Severe inflammatory infiltrates containing eosinophils were observed in
810 the lungs of the UV-V-immunized mouse (A, inset). A few virus antigens were present in the
811 bronchi (B). The UV-V+Alum-immunized mouse also showed eosinophilic inflammatory
812 reactions, but no viral antigen-positive cells were present in the lungs (C, inset and D).
813 Congestion, hemorrhage, and pulmonary edema with mononuclear cell infiltration were observed
814 in the mock vaccinated mouse (PBS+Alum) (E, inset). Cells positive for viral antigen were seen

815 throughout the lung (F). Hematoxylin and eosin (magnification, 10×) and C.M.E kit staining
816 (inset, magnification, 100×), a reliable and specific stain for eosinophils (A, C, and E).
817 Immunohistochemical staining with an anti-SARS-CoV antibody (magnification, 20×, B, D, and
818 F).
819
820 **Figure 3. Reinfection of SARS-CoV in aged mice.** Aged mice were infected with the
821 HKU39849 isolate or mock vaccinated (no vaccination) and subsequently infected with 1000
822 $TCID_{50}$ of F-musX. (A) Mice were weighed daily after challenge. All mock vaccinated mice died
823 by day 5, but all reinfected mice survived. Dead mice are marked with crosses. Error bars
824 indicate standard deviation. (B) Virus titers in the lungs and lung wash fluids 3 days after
825 challenge (n = 3). The dashed line indicates the limit of detection ($10^{1.5}$ $TCID_{50}$/ml). Error bars
826 indicate standard deviation. Significant between group differences ($p < 0.05$ by one-way
827 ANOVA) are marked with an asterisk. (C) Neutralizing serum antibody titers against SARS-CoV
828 on days 0, 3, and 10 after challenge (n = 6-12). Serum samples were 2-fold serially diluted
829 beginning at 1:2. Error bars indicate standard deviation. Significant between group differences (p
830 < 0.05 by one-way ANOVA) are marked with an asterisk. (D) Numbers of lymphocytes,

macrophages, neutrophils, and eosinophils in lung sections (n = 3) 3 days after challenge. Five 240 μm^2 regions in the extrabronchioles of each mouse lung were examined at 40× magnification. Asterisks indicate p <0.05 by the Bonferroni test. Error bars indicate standard deviation. (E) Representative images of the lungs of SARS-CoV reinfected mice. Br, bronchi; *, blood vessel. Lung samples taken 3 and 10 days after infection were sectioned and stained with hematoxylin and eosin (magnification, 10×) and the C.E.M. kit (inset, magnification, 100×).

Figure 4. Immunization with UV-V and TLR agonists inhibits excessive eosinophilic infiltration after SARS-CoV challenge. Adult female BALB/c mice were vaccinated with UV-V, UV-V with TLR agonists (UV-V+TLR), or vehicle (PBS) and subsequently challenged with 1000 $TCID_{50}$ of F-musX. Dead mice are marked with crosses. (A and B) Mice were weighed daily and monitored for morbidity (n = 6–7). (C) SARS-CoV titers in the lungs and lung wash fluids 3 days after intranasal challenge with SARS-CoV (n = 4). Significant differences (p < 0.05, one-way ANOVA) between groups are marked with an asterisk. The dashed line indicates the limit of detection ($10^{1.5}$ $TCID_{50}$/ml). Error bars indicate standard deviation. (D) SARS-CoV-specific neutralizing serum antibody titers 52, 10, and 0 days before challenge (n =

13–14) and 3 and 10 days after challenge with SARS-CoV (n = 6-7, respectively). Serum samples were 2-fold serially diluted beginning at 1:2. Error bars indicate standard deviation. (E) Representative images of lung sections from mice immunized with UV-V, UV-V+LPS, or UV-V+TLR on days 3 and 10 after challenge with F-musX. Hematoxylin and eosin (magnification, x10) and C.E.M. kit staining (inset, magnification, 100×). Br, bronchi; *, blood vessel. (F) Numbers of lymphocytes, macrophages, neutrophils and eosinophils in the lung sections (n = 3). Five 240-μm^2 regions in the extrabronchioles of lung per mouse were examined at 40× magnification. Asterisks indicate p <0.05 by the Bonferroni test. Error bars indicate standard deviation.

Figure 5. Cytokine and chemokine protein concentrations in lung homogenates of mice immunized with UV-V and challenged with SARS-CoV.

The concentrations of cytokines and chemokines in lung homogenates were determined on days 3 and 10 after challenge (n = 4). Asterisks indicate significant differences (P < 0.05, one-way ANOVA). Error bars indicate standard deviation.

863 **Figure 6. Type I IFN gene expression in lung homogenates of mice immunized with UV-V**
864 **and challenged with SARS-CoV.** (A) Type I IFN mRNA expression profiles in UV-V- and
865 UV-V+TLR-immunized mice, and (B) amounts of viral RNA present during infection. RNA was
866 taken from the lungs of UV-V- and UV-V+TLR-immunized mice 1 day after challenge. Type I
867 IFN mRNAs and SARS-CoV genome (nsp11 region) were measured by quantitative real-time
868 RT-PCR. Results are expressed as $\log_{10}$ fold-change compared with mock-vaccinated, challenged
869 mice. *, $P < 0.05$. Error bars indicate standard deviations.
870
871 **Figure 7. Immunization with UV-V or UV-V+TLR induces eosinophilic immune pathology**
872 **in adult mice after long-term SARS-CoV challenge.** Adult female BALB/c mice were
873 vaccinated with UV-V or UV-V+TLR or mock vaccinated (PBS), and subsequently challenged
874 with 1000 $TCID_{50}$ of F-musX. (A) Body weight changes following the challenge inoculation (n =
875 7). Dead mice are marked with crosses. Error bars indicate the standard deviation. (B) Virus titers
876 in the lungs and lung wash fluids on day 3 post-challenge (n = 4). The dashed line indicates the
877 limit of detection ($10^{1.5}$ $TCID_{50}$/ml). Error bars indicate standard deviation. Significant between
878 group differences ($p < 0.05$ by one-way ANOVA) are marked with an asterisk. (C) Neutralizing

879 serum antibody titers against SARS-CoV 1 day before challenge (n = 14), and 3 and 10 days after
880 challenge (n = 7 each). Serum samples were 2-fold serially diluted beginning at 1:2. Error bars
881 indicate standard deviation. Significant between group differences ($p < 0.05$ by one-way
882 ANOVA) are marked with an asterisk. (D) Numbers of lymphocytes, macrophages, neutrophils
883 and eosinophils in lung sections (n = 3). Five 240 μm^2 regions in the extrabronchioles in the
884 lungs of each mouse were examined at 40× magnification. Asterisks indicate $p < 0.05$ by the
885 Bonferroni test. Error bars indicate standard deviation. (E) Representative images of lung
886 sections from UV-V (left panel)- and UV-V+TLR (right panel)-immunized mice 3 days after
887 challenge. Hematoxylin and eosin (magnification, 10×) and C.E.M. kit staining (inset,
888 magnification, 100×). Br, bronchi; *, blood vessel.
889
890 **Figure 8. Global gene expression profiles of mice immunized with UV-V after SARS-CoV**
891 **challenge.** An ANOVA was performed to assess differences among all groups. All genes with a
892 greater than 2.0-fold change ($P < 0.05$) in expression, relative to the median of the unchallenged
893 groups, are depicted. Each row represents the lungs of a group of mice (n = 3, mock
894 immunization with PBS (PBS); n = 6, inoculation with HKU39849 isolate (HKU), UV-V (UVV)

895 or UV-V+TLR (UVVTLR)). The heat map shows the relative levels of expression of 305 probes
896 (242 genes), confirmed statistically by direct comparisons between the UV-V and UV-V+TLR
897 groups. The heat map was generated using the software GeneSpring GX 12.1. (A) Uncentered
898 Pearson correlation was used as the distance metric with average linkage for unsupervised
899 hierarchical clustering. In the heatmap, red represents high expression, black represents median
900 expression, and green represents low expression. The color scale bar at the bottom indicates the
901 relative level of expression. The sidebar on the right indicates genes that are closely related to
902 each other. (B) A gene interaction network including 39 genes was constructed from 242 genes
903 connected by IPA software. The solid and dotted lines indicate direct and indirect interactions,
904 respectively. Genes shown in red were up-regulated and those shown in green were
905 down-regulated, compared with the PBS group. The central node is IL-4, a key cytokine in
906 inflammation associated with eosinophils. Network 1 was composed of genes associated with
907 eosinophilia. Network 2 was composed of genes associated with " inflammation of the lungs".
908 The same network is shown for UV-V- (upper panel) and UV-V+TLR-immunized (lower panel)
909 mice.
910

911 **Figure 9. A network of genes in mice immunized with UV-V after SARS-CoV challenge.**
912 Direct comparison of gene expression profiles in the lungs of UV-V- and
913 UV-V+TLR-immunized mice. Diagram showing the TLR3 and TLR4 signaling pathways. Genes
914 shown in red were up-regulated and those in green were down-regulated, compared with the PBS
915 group. Several genes downstream of TLR3 and TLR4 signaling were up-regulated in
916 UV-V+TLR- (lower panel) compared with UV-V-immunized (upper panel) mice. We overlaid
917 gene expression data on the formed network using Ingenuity Pathway Analysis software.
918
919 **Figure 10. Pathway analysis of the gene-to-gene networks of TLR3, TLR4 and polyI:C in**
920 **mice immunized with UV-V after SARS-CoV challenge.** Direct comparison of gene
921 expression profiles in CD11b+ cells isolated from the lungs of UV-V- and
922 UV-V+TLR-immunized mice. (A, D) FACS analysis of enriched populations of CD11b+ lung
923 cells in UV-V (A) and UV-V+TLR (D) immunized mice. Cells were prepared as described in the
924 Materials and Methods. (B, E) Conventional Giemsa staining of cytospins from populations of
925 CD11b+ lung cells in UV-V (B) and UV-V+TLR (E) immunized mice (magnification: 100x). (C,
926 F) Diagram showing the pathways of TLR3 and TLR4 signaling. Genes shown in red were

927 up-regulated and those in green were down-regulated. Several genes downstream of TLR3 and
928 TLR4 signaling were up-regulated in UV-V (C) compared with UV-V+TLR (F) immunized mice.
929 We overlaid gene expression data on the formed network by Ingenuity Pathway Analysis
930 software.
931
932
933
934
935

Figure 1

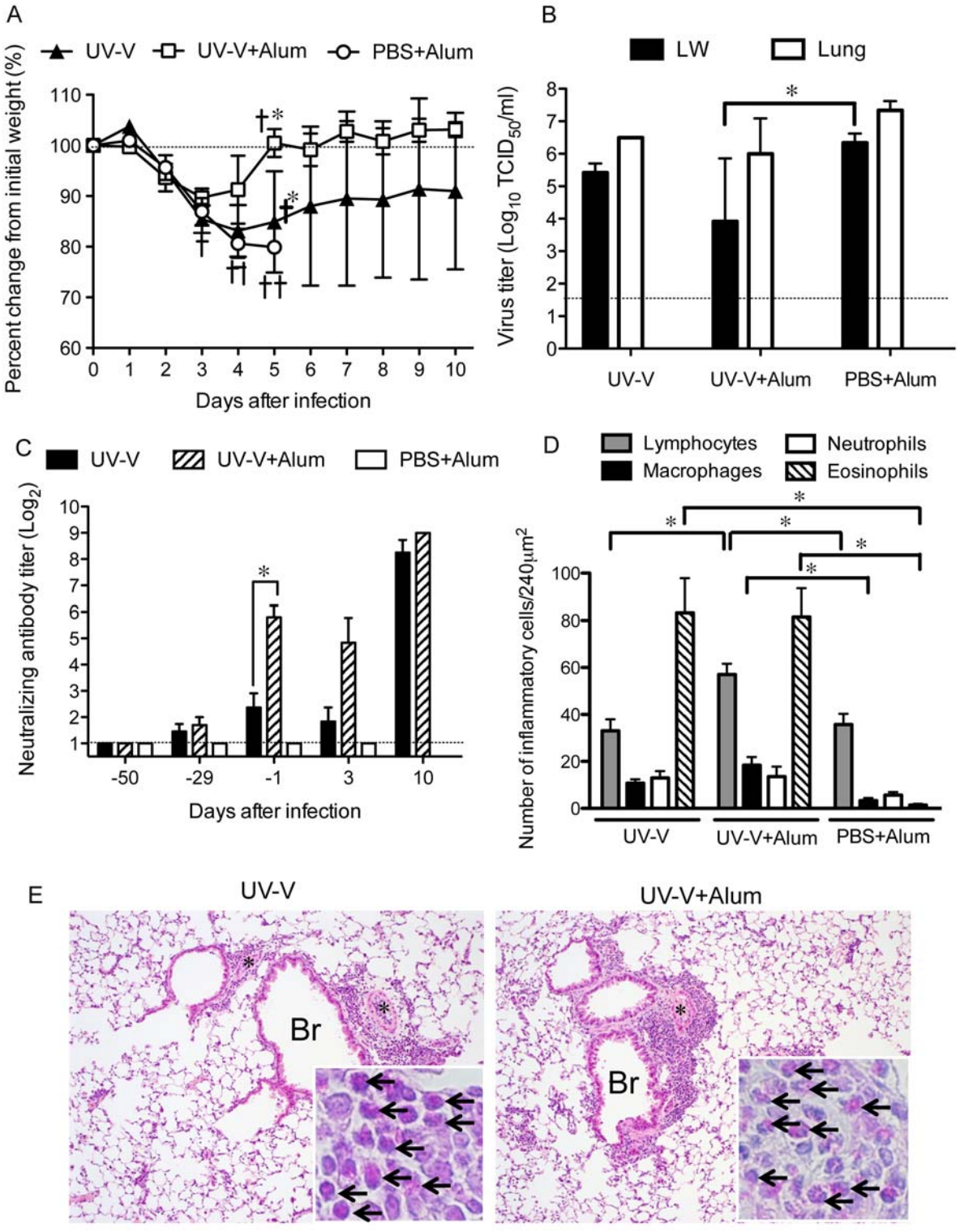

Figure 2

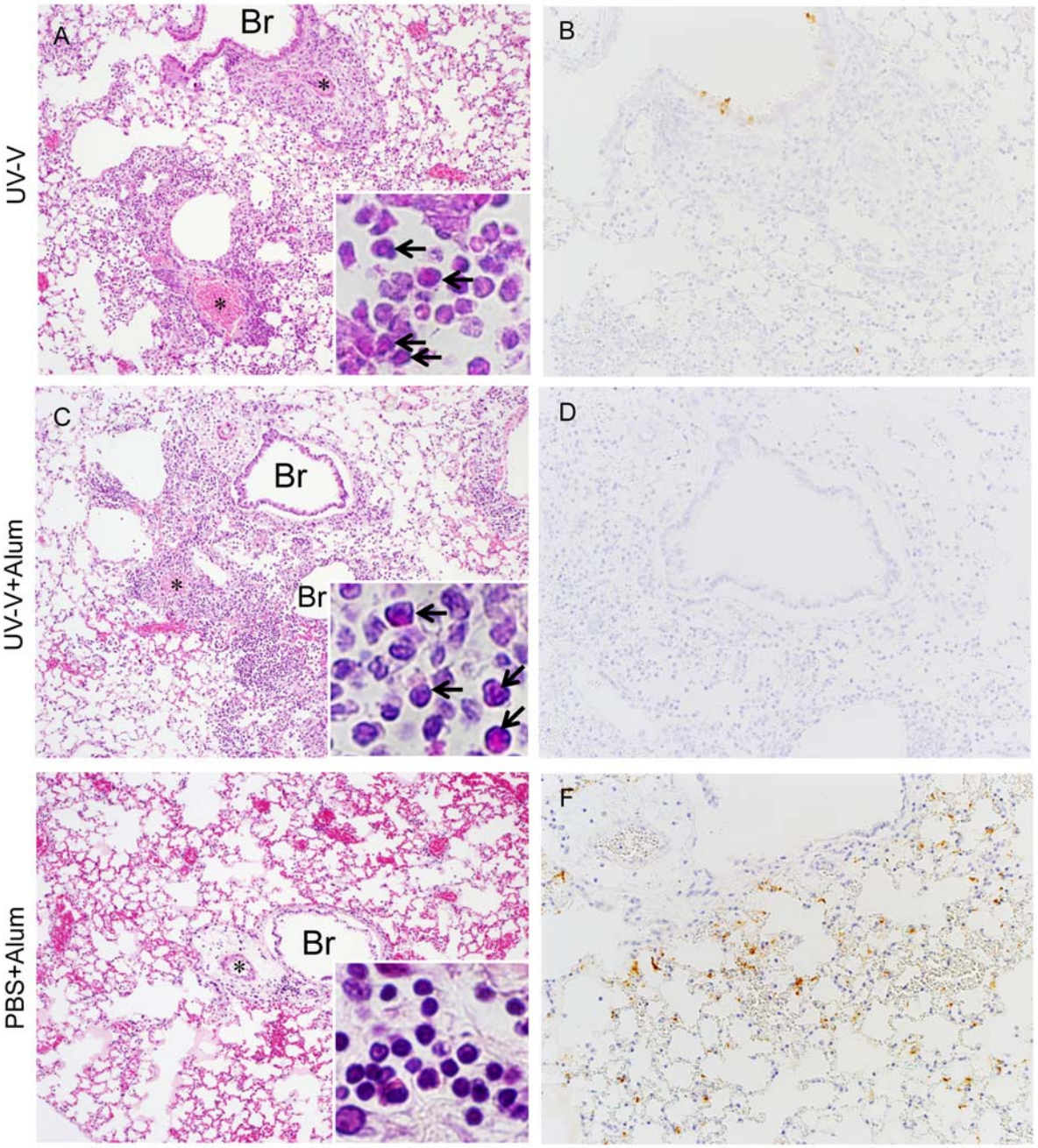

Figure 3

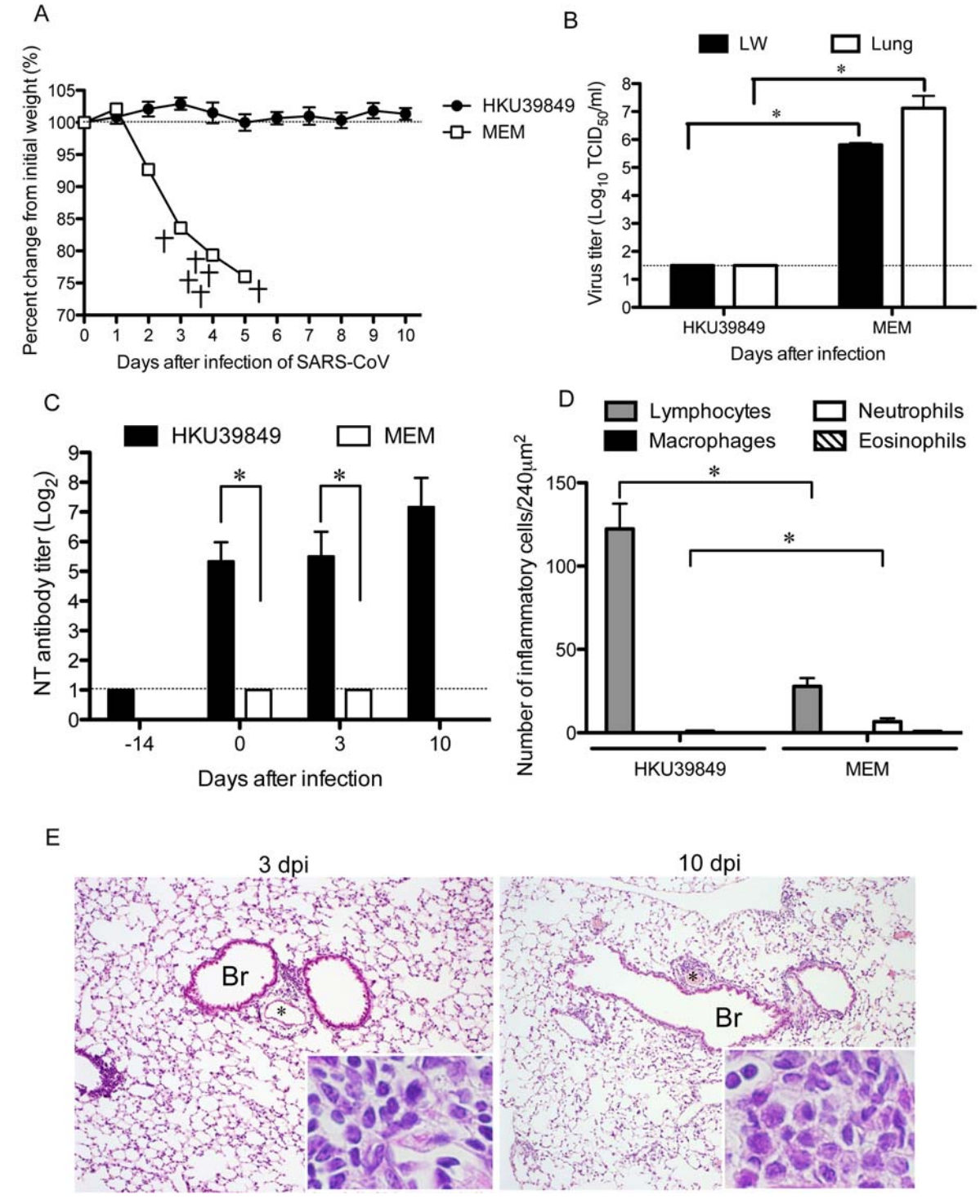

Figure 4

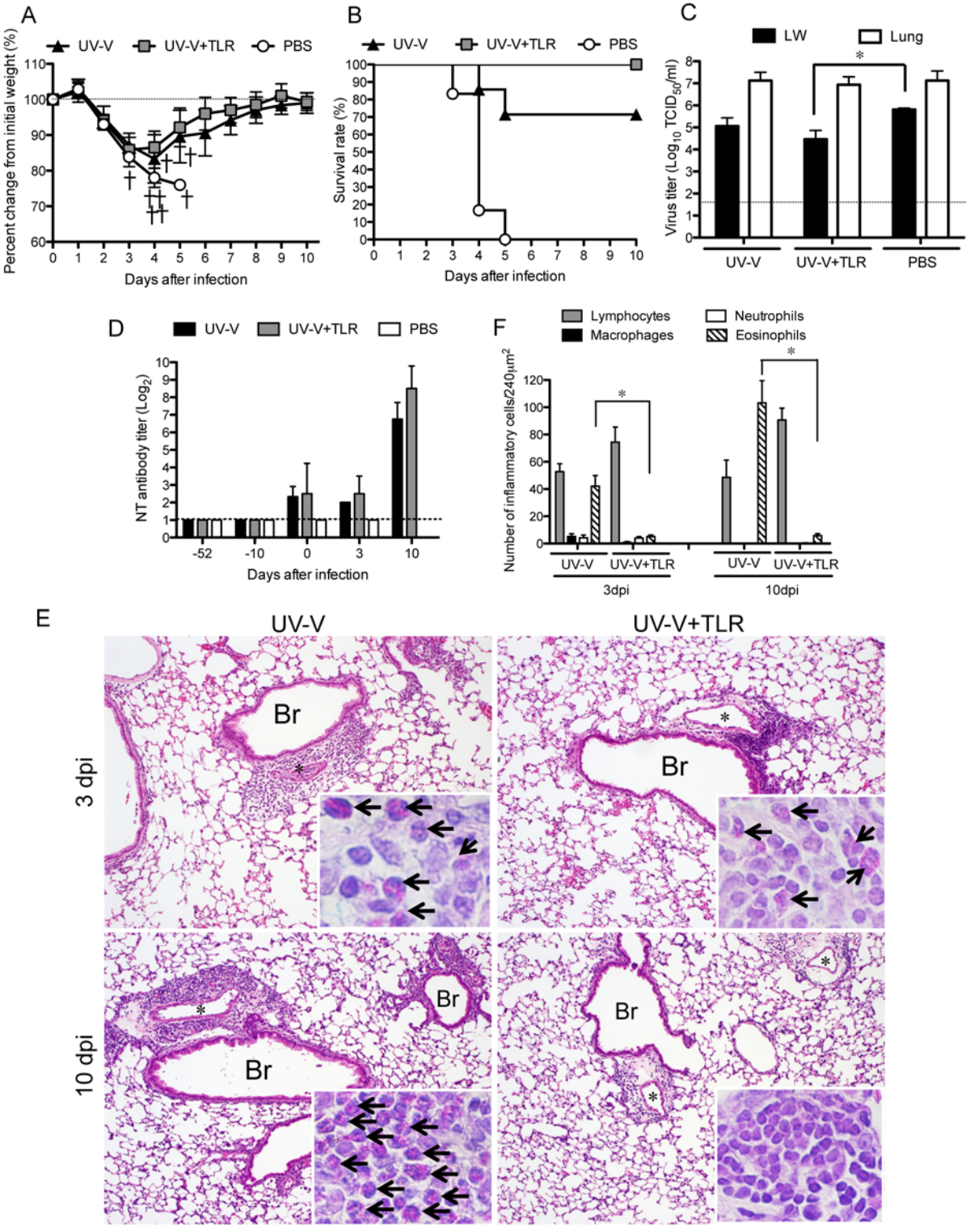

Figure 5

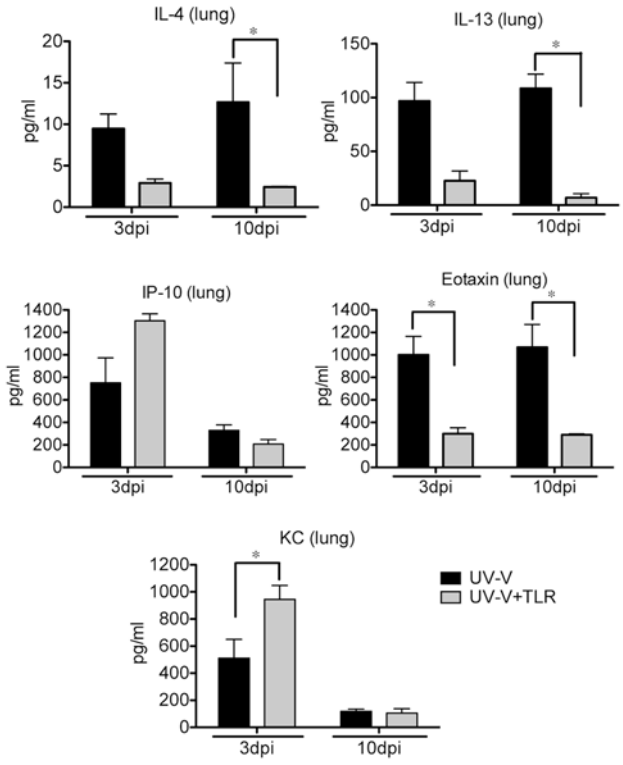

Figure 6

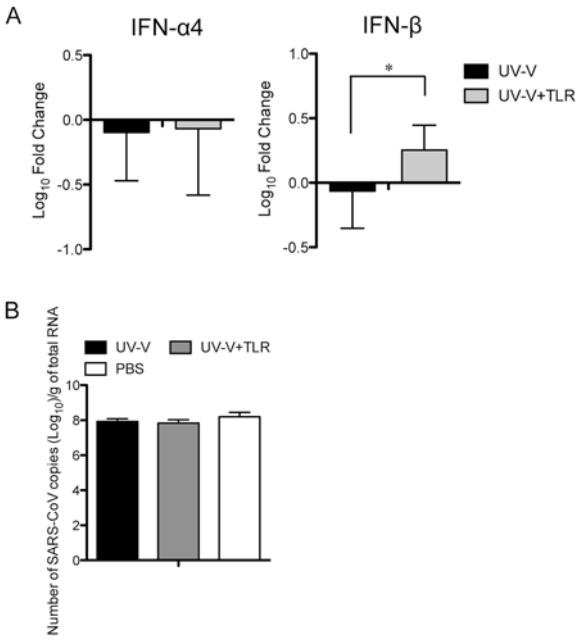

Figure 7

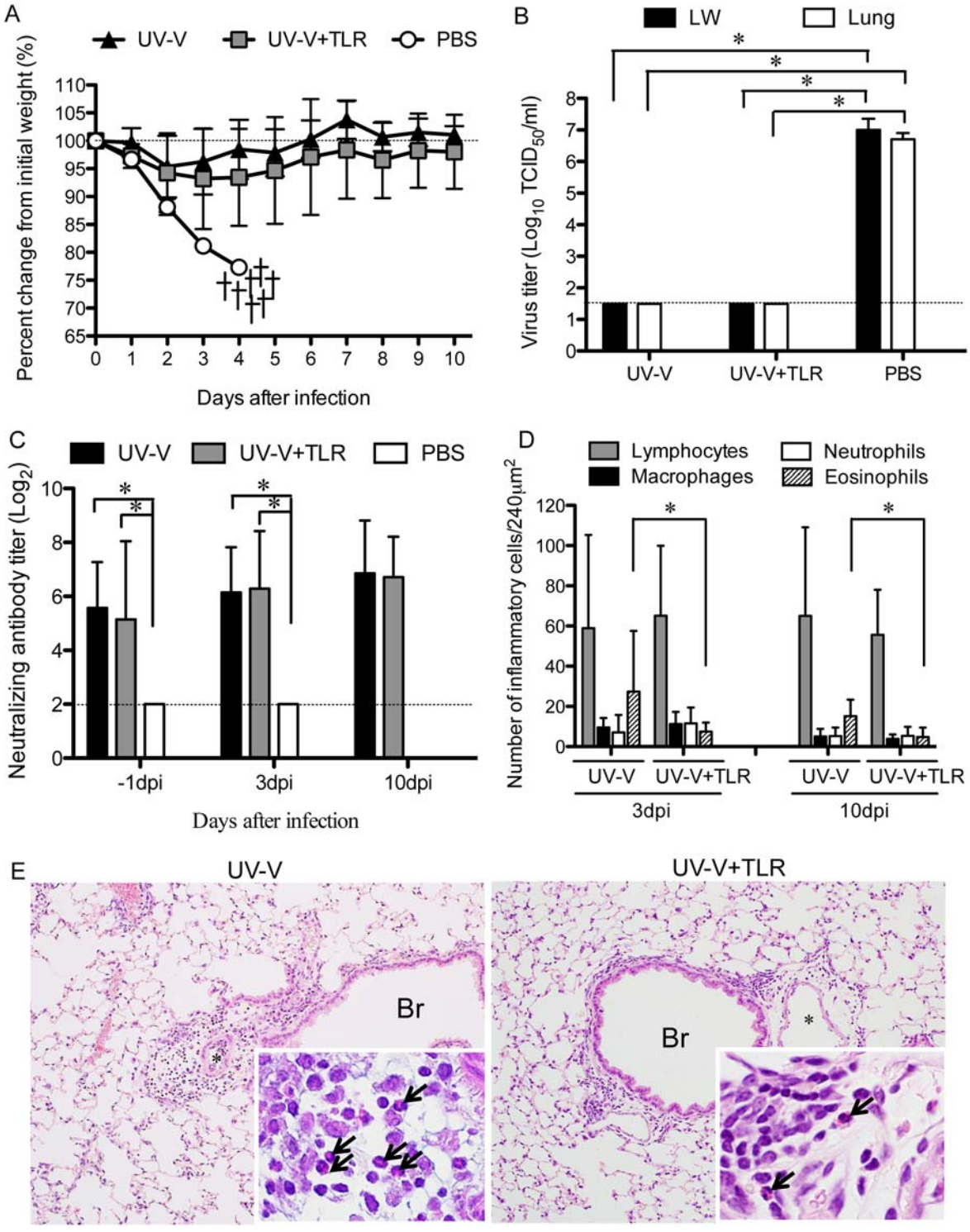

Figure 8

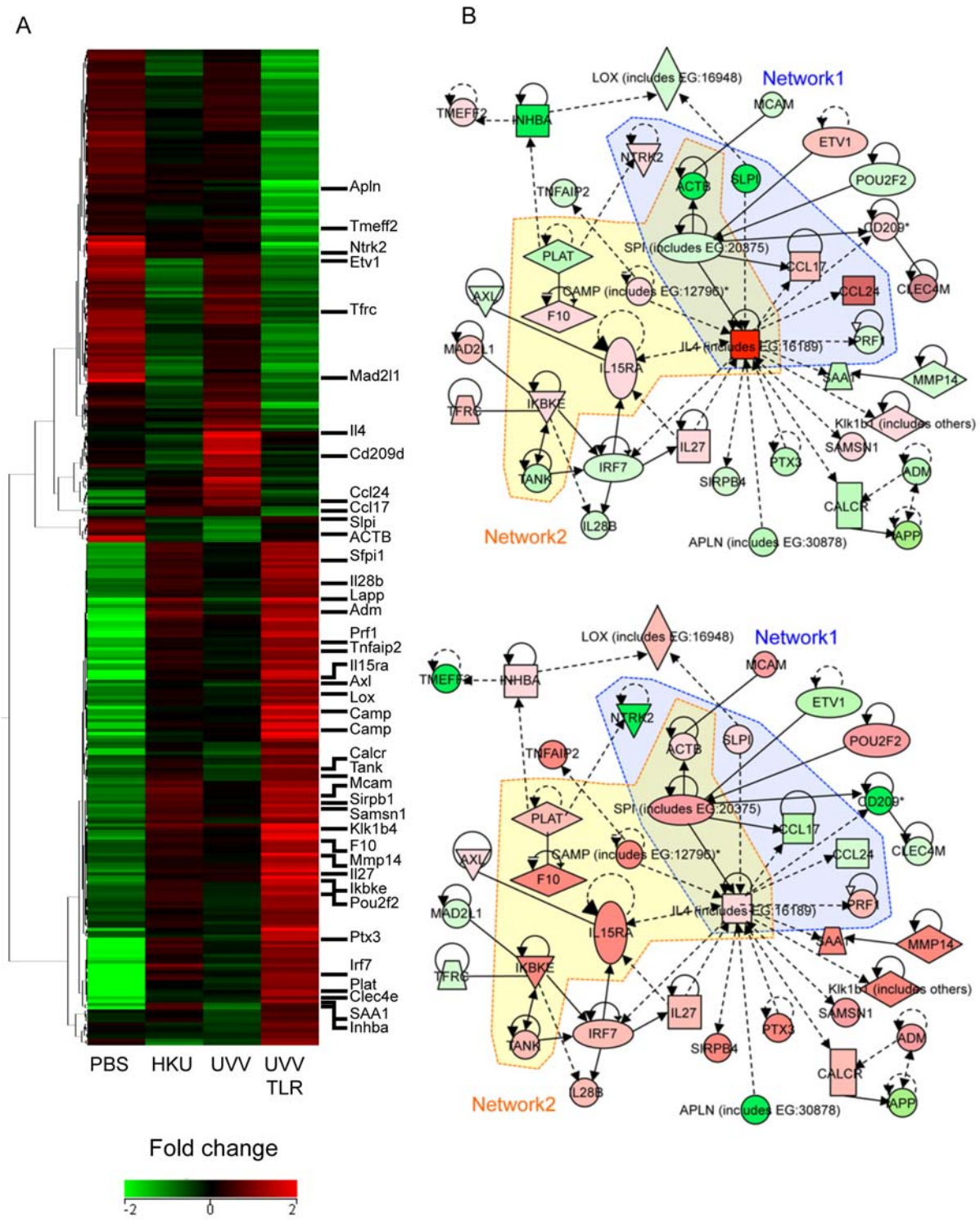

Figure 9

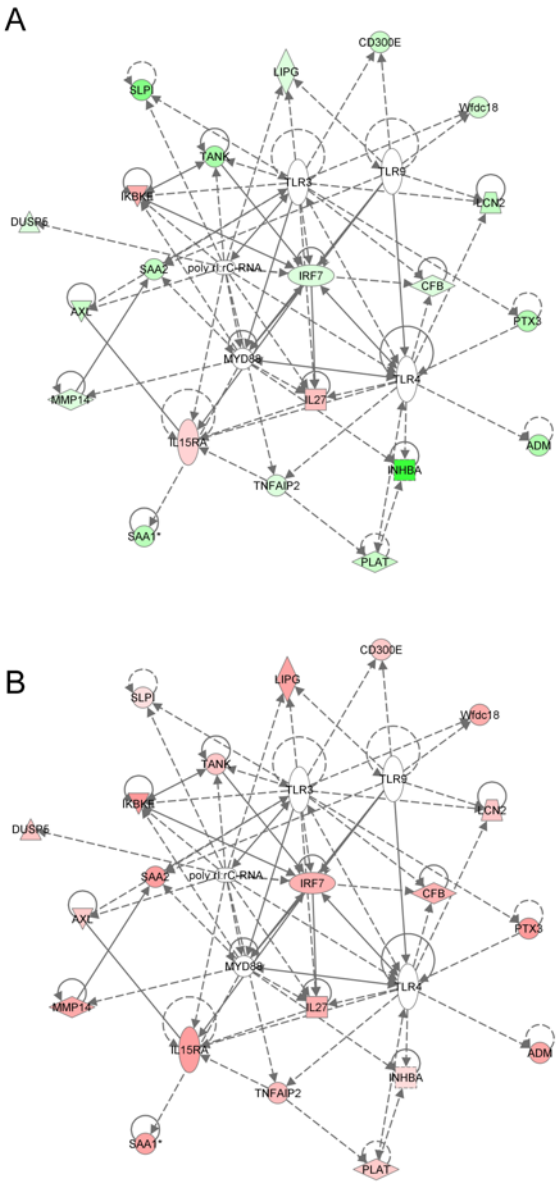

Figure 10